

Whitecap coverage from satellite measurements: A first step toward modeling the variability of oceanic whitecaps

Magdalena D. Angelova^{1,2} and Ferris Webster¹

Received 11 July 2005; revised 17 August 2005; accepted 25 November 2005; published 24 March 2006.

[1] We present estimates of whitecap coverage on a global scale from satellite-measured brightness temperature of the ocean surface. This is a first step in a larger framework aiming at more realistic modeling of the high variability of whitecap coverage as a function of wind speed and a suite of additional environmental and meteorological factors. The involvement of oceanic whitecaps in various physical and chemical processes important for climate studies such as production of sea-salt aerosols, enhancement of air-sea gas exchange, and influence on retrievals of ocean surface wind and ocean color motivates this effort. A critical review of the physical variables causing the high variability of whitecap coverage and existing approaches modeling this variability establishes the need for a database of whitecap coverage and concomitant measurements of additional factors. The necessity to build such an extensive database justifies the quest for a method estimating whitecap coverage from satellite data. We describe the physical concept, a possible implementation, error analysis, results, and evaluation of a method for estimating whitecap coverage from routine satellite measurements. The advantages of the concept and the drawbacks and necessary improvements of the implementation are discussed.

Citation: Angelova, M. D., and F. Webster (2006), Whitecap coverage from satellite measurements: A first step toward modeling the variability of oceanic whitecaps, *J. Geophys. Res.*, *111*, C03017, doi:10.1029/2005JC003158.

1. Introduction

[2] Breaking waves in the ocean entrain air into seawater forming clouds of bubbles beneath and foamy patches on the sea surface. The fraction of the ocean surface covered with sea foam and mixed with bubbles is defined as whitecap coverage (or foam fraction), W . The global average has been cited to be 1–4% [Blanchard, 1963, 1983]. Whitecap coverage is usually modeled as a function of wind speed at 10-m reference height above the sea surface, U_{10} . However, it exhibits high variability, which cannot be predicted with the wind alone. Various environmental and meteorological factors in addition to wind influence it [Williams, 1969; Monahan and O’Muircheartaigh, 1986].

[3] Whitecaps mark places in the ocean where various physical processes are either enhanced or completely different from those in and on surrounding seawater. Through these physical and many consequent chemical processes, oceanic whitecaps are directly and indirectly involved in the climate system. Inadequate modeling of the high variability of whitecap coverage introduces uncertainty in the model-

ing of all air-sea processes correlated with W . The importance of whitecap coverage for climate studies motivates the work presented here. The list below of air-sea processes associated with whitecaps justifies our efforts.

[4] Oceanic whitecaps mark areas actively producing sea spray droplets via bubble bursting (film and jet droplets) and via the wind tearing off wave crests (spume droplets) [Blanchard, 1983; Wu, 1992a; Andreas et al., 1995]. Sea spray droplets with sizes above 1 μm alter interfacial fluxes of sensible and latent heat by as much as 15 and 150 Wm^{-2} , respectively [Andreas et al., 1995]. About half of these fluxes would be available to the entire boundary layer [Fairall et al., 1994], making it necessary to include them in Earth’s heat budget. On a more regional scale, the relatively large sea spray droplets affect tropical cyclone intensity [Fairall et al., 1994; Andreas and Emanuel, 2001]. Smaller sea spray droplets, with sizes below 20 μm , reside in the air long enough to reach moisture equilibrium [Andreas, 1992] and transform into sea-salt aerosols [Blanchard, 1983]. Sea-salt aerosols have the potential to mitigate global warming directly by increasing planetary albedo [Haywood et al., 1999; Winter and Chylek, 1997; Jacobson, 2001; Takemura et al., 2002; Grini et al., 2002; Liao et al., 2004], indirectly by acting as cloud condensation nuclei (CCN) thus altering cloud albedo [Andreae, 1995; O’Dowd et al., 1997, 1999; Ghan et al., 1998], and chemically by removing methane and surface ozone, both potent greenhouse gases, from the atmosphere [Barrie et al., 1988; Keene et al., 1990; Sander and Crutzen, 1996; Finlayson-Pitts and Pitts, 1997; Koop et al., 2000; Liao et

¹College of Marine Studies, University of Delaware, Lewes, Delaware, USA.

²Now at Naval Research Laboratory, Washington, DC, USA.

al., 2004]. Under certain conditions, sea-salt aerosols may diminish the cooling effect of the sulfate aerosols predicted by the *Charlson et al.* [1987] hypothesis by rapid removing of natural and anthropogenic sulfates from the atmosphere and by preventing the activation of sulfate aerosols as CCN [*Luria and Sievering*, 1991; *Chameides and Stelson*, 1992; *Sievering et al.*, 1992, 1995; *Clegg and Toumi*, 1998; *Liao et al.*, 2004]. For all these reasons, the processes involving sea spray must be adequately parameterized and included in climate models. The first step in modeling sea spray droplets is their generation, and in most cases the sea spray source function requires whitecap coverage [*Andreas*, 2002].

[5] Oceanic whitecaps mark areas of enhanced air-sea gas exchange. Accurate estimates of air-sea gas fluxes are essential for understanding the global biogeochemical cycles of CO₂, CH₄, NO_x, DMS and other trace gases that affect Earth's radiation budget [*Frew*, 1997]. Parameterizations of the transfer velocity of various gases across the air-sea interface [*Monahan and Spillane*, 1984; *Liss and Merlivat*, 1986; *Tans et al.*, 1990; *Wanninkhof*, 1992; *Asher and Wanninkhof*, 1998; *Asher et al.*, 2002] require a knowledge of whitecap coverage.

[6] Oceanic whitecaps mark areas with increased surface emission and brightness temperature at microwave frequencies [*Ross et al.*, 1970; *Williams*, 1971; *Smith*, 1988a; *Swift*, 1990]. Together with the surface roughness, they are a key component of the signal used to obtain surface wind vector with satellite-borne radiometric and polarimetric instruments [*Wentz*, 1997; *Yueh*, 1997; *Gaiser et al.*, 2004]. The global wind vector field is one of the initializing variables in climate models whose requirements for accuracy constantly increase. The accuracy of wind vector retrievals from physically based algorithms may improve if the geophysical model function includes foam emissivity and whitecap coverage.

[7] Oceanic whitecaps mark areas with high reflectance at visible frequencies [*Gordon and Jacobs*, 1977; *Koepke*, 1986; *Stabenro and Monahan*, 1986; *Kokhanovsky*, 2004]. Since their presence increases ocean surface and planetary albedos, it must be accounted for in models evaluating the global radiation budget [*Frouin et al.*, 2001]. In addition, because sea foam masks the water-leaving radiance used to retrieve ocean color and primary production [*Gordon and Wang*, 1994; *Moore et al.*, 2000], its effect must be corrected accordingly using whitecap coverage.

[8] Including parameterizations of all these processes in climate models requires an estimation of global whitecap coverage. Currently, global whitecap coverage is estimated by combining a global wind field, U_{10} , obtained from satellite-borne radiometers or scatterometers, and an empirical relation, $W(U_{10})$. However, to obtain more accurate predictions of whitecap coverage, a model of W must account for its dependence on a suite of additional factors. To investigate correlations and develop physically sound models for these additional dependences, a database of whitecap coverage under various environmental and meteorological conditions is necessary. Since the existing photographic measurements of whitecap coverage are not enough to organize an adequate database of W with concomitant measurements of environmental and meteorolog-

ical variables, an alternative approach for measuring whitecap coverage is in order.

[9] This paper documents results on the first step in this framework, namely estimating whitecap coverage on a global scale from satellite-measured brightness temperature of the ocean surface. Building on the existing knowledge of oceanic whitecaps, section 2 justifies the quest for a new way of measuring whitecap coverage by demonstrating its high variability, identifying the factors causing this high variability, reviewing the existing approaches of modeling it, and establishing the need for an extensive database of whitecap coverage and accompanying variables. Section 3 presents briefly the physical concept, implementation, and error analysis of a method estimating W from routine satellite measurements. Section 4 reports results on satellite-based estimates of whitecap coverage and evaluates them. Finally, section 5 discusses the advantages of the concept and the drawbacks and necessary improvements of the described implementation.

2. Oceanic Whitecaps

2.1. Whitecap Coverage Variability

[10] The lowest wind speed at which whitecaps may appear is around 3 m s^{-1} [*Monahan and O'Muircheartaigh*, 1986; *Hanson and Phillips*, 1999]. Certainly, wind speed is the main cause for the formation of whitecaps and both oceanographic and remote sensing communities have proposed many empirical expressions for the $W(U_{10})$ relation, each developed as the best fit to data set(s) at specific locations and conditions. These various parameterizations are summarized in Table 1 and plotted in Figure 1. With a few exceptions, most of the proposed $W(U_{10})$ expressions are a power law in the form aU_{10}^b with b typically around 3 or $a(U_{10}-c)^3$ with c loosely associated with the threshold wind speed for whitecap formation under the specific conditions of the measurements. This functional form of $W(U_{10})$ conforms to *Cardone's* [1969, pp. 64–69] (also discussed by *Monahan* [1971]) suggestion that whitecaps manifest the dissipation of excessive energy transferred from the air flow to the waves. *Wu* [1979, 1988, 1992b] expressed this on dimensional grounds as whitecap coverage, W , proportional to the cube of wind specified either in terms of friction velocity u_* or wind at reference height z , U_z , e.g., $W \sim u_*^3 \sim U_z^3$. Though measurements roughly confirm this physically sound conclusion, there are wide variations from one parameterization to another: the exponent b ranges from 1 (*Bortkovskii* [1987], cold waters) to above 5 [*Hanson and Phillips*, 1999] and the threshold wind speed c is from 0.6 m s^{-1} [*Reising et al.*, 2002] to above 6 m s^{-1} (*Stramska and Petelski* [2003], undeveloped sea). Different values for b or c quantify different water temperatures (cold, moderate, warm), atmospheric stability (neutral, stable, unstable), or wind fetch and duration (developed, undeveloped sea) regimes. Figure 1 clearly demonstrates the wide variability of whitecap coverage, especially at low and moderate winds. This is upward of 3 orders of magnitude variability for winds of 5 m s^{-1} , and nearly 2 orders of magnitude variability for winds of 10 m s^{-1} . Such a high variability implies that other factors, beside the wind, are at play and models in terms

Table 1. Parameterizations of Whitecap Coverage as a Function of Wind Speed^a

Data Set Number	Reference	Name in Figure 1	Formula	Notes
1	Monahan [1971]	Monahan '71	$W = 1.35 \times 10^{-3} U_{10}^{3.4}$	in percent $U_{20} \geq 7 \text{ m s}^{-1}$
2	Wilheit [1979]	Wilheit '79	$W = a(1 - e^{-bW})(U_{20} - 7)$, $a = 0.006 \text{ s m}^{-1}$, $f_0 = 7.5 \text{ GHz}$	
3	Monahan and O'Muircheartaigh [1980]	M&O'M '80 RBF	$W = 3.84 \times 10^{-6} U_{10}^{3.44}$	
4	Monahan and O'Muircheartaigh [1980]	M&O'M '80 OLS	$W = 2.95 \times 10^{-6} U_{10}^{3.52}$	
5	Bondur and Sharkov [1982]	Bondur&Sharkov '82 A	$W = 0.015[1 + 2.2 \times 10^{-2}(U_{19.5} - 5)^3]$	in percent, $U_{19.5} \geq 5 \text{ m s}^{-1}$
6	Bondur and Sharkov [1982]	Bondur&Sharkov '82 B	$W = 0.65[1 + 4.76 \times 10^{-2}(U_{19.5} - 5)^2]$	In %, $U_{19.5} \geq 5 \text{ m s}^{-1}$
7	Pandey and Kakar [1982]	Pandey&Kakar 82	$W = b_0 + b_1 U_{10} + b_2 U_{10}^2$ $b_0 = 1.707 \times 10^{-2} + 8.560 \times 10^{-4} F + 1.12 \times 10^{-5} F^2$ $b_1 = -1.501 \times 10^{-2} + 1.821 \times 10^{-3} F - 4.634 \times 10^{-5} F^2$ $b_2 = 2.442 \times 10^{-4} - 2.282 \times 10^{-6} F + 4.194 \times 10^{-7} F^2$	using SMMR data, F [GHz]
8	Monahan et al. [1983a]	Monahan et al. '83	$W = 4.5 \times 10^{-6} U_{10}^{3.31}$	
9	Spillane et al. [1986]	Spillane et al '86 cold	$W = 9.279 \times 10^{-5} U_{10}^{2.112}$	
10	Spillane et al. [1986]	Spillane et al '86 moder.	$W = 4.755 \times 10^{-5} U_{10}^{3.525}$	
11	Spillane et al. [1986]	Spillane et al '86 warm	$W = 3.301 \times 10^{-6} U_{10}^{3.479}$	
12	Monahan and O'Muircheartaigh [1986]	M&O'M 86 $dT_s = 0$ (neutral)	$W = 1.95 \times 10^{-5} U_{10}^{2.55} \exp(0.0861 \cdot \Delta T_s)$	
13	Borkovskii [1987]	Bork'87, A + B, cold	$W = 0.189 U_{10} - 1.28$	in percent, his Table 2.1
14	Borkovskii [1987]	Bork'87, A + B, moder	$W = 1.71 \times 10^{-5} U_{10}^{4.443}$	in percent, his Table 2.1
15	Borkovskii [1987]	Bork'87, A + B, warm	$W = 6.78 \times 10^{-3} U_{10}^{0.76}$	in percent, his Table 2.1
16	Wu [1988]	Wu '88	$W = 1.7 \times 10^{-6} U_{10}^{3.75}$	
17	Monahan and Woolf [1989]	Mon&W'89, A, $dT_s = 0$ (ntrl)	$W = 2.92 \times 10^{-7} U_{10}^{3.204} \exp(0.1198 \cdot \Delta T_s)$	
18	Monahan [1993]	Monhan'93 visc., A	$W = 1.98 \times 10^{-12} \nu^{-1} (U_{10} - 2.22 \times 10^{2 \cdot \nu^{1/3}})^3$	ν kinematic viscosity
19	Monahan [1993]	Monhan'93 visc., B	$W = 1.44 \times 10^{-11} \nu^{-1} (U_{10} - 1.62 \times 10^{2 \cdot \nu^{1/3}})^3$	ν kinematic viscosity
20	Asher and Wanninkhof [1998]	Asher&Wann'98, A	$W = 2.56 \times 10^{-6} (U_{10} - 1.77)^3$	
21	Hanson and Phillips [1999]	Hanson&Phillips '99, no \lll	$W = 2.04 \times 10^{-7} U_{10}^{3.61}$	exclude measurements with $W < 5 \times 10^{-5}$
22	Hanson and Phillips [1999]	Hanson&Phillips '99, all meas	$W = 3.66 \times 10^{-9} U_{10}^{5.16}$	all measurements considered
23	Asher et al. [2002]	Asher et al. '02, A	$W = 3.7 \times 10^{-6} (U_{10} - 1.2)^3$	
24	Reising et al. [2002]	Reising et al. '02, A	$W = 3.5 \times 10^{-6} (U_{10} - 0.6)^3$	
25	Sramaska and Petelski [2003]	Sram&Petel'03 tot	$W = 4.18 \times 10^{-5} (U_{10} - 4.93)^3$	all W measured
26	Sramaska and Petelski [2003]	Sram&Petel'03 dev.	$W = 5.0 \times 10^{-5} (U_{10} - 4.47)^3$	developed sea
27	Sramaska and Petelski [2003]	Sram&Petel'03 undev.	$W = 8.75 \times 10^{-5} (U_{10} - 6.33)^3$	undeveloped sea
28	Villarino et al. [2003]	Villarino et al '03, stable	$W = 2.32 \times 10^{-6} U_{10}^{3.4988}$	stable conditions
29	Villarino et al. [2003]	Villarino et al '03, unst.	$W = 0.43 \times 10^{-6} U_{10}^{3.6824}$	unstable conditions
30	Lafon et al. [2004]	Lafon et al., 2004	$W = 1.51 \times 10^{-4} U_{10}^{6.65}$	In %, $U_{10} > 5 \text{ m s}^{-1}$

^a W values are reported as a fraction unless otherwise specified.

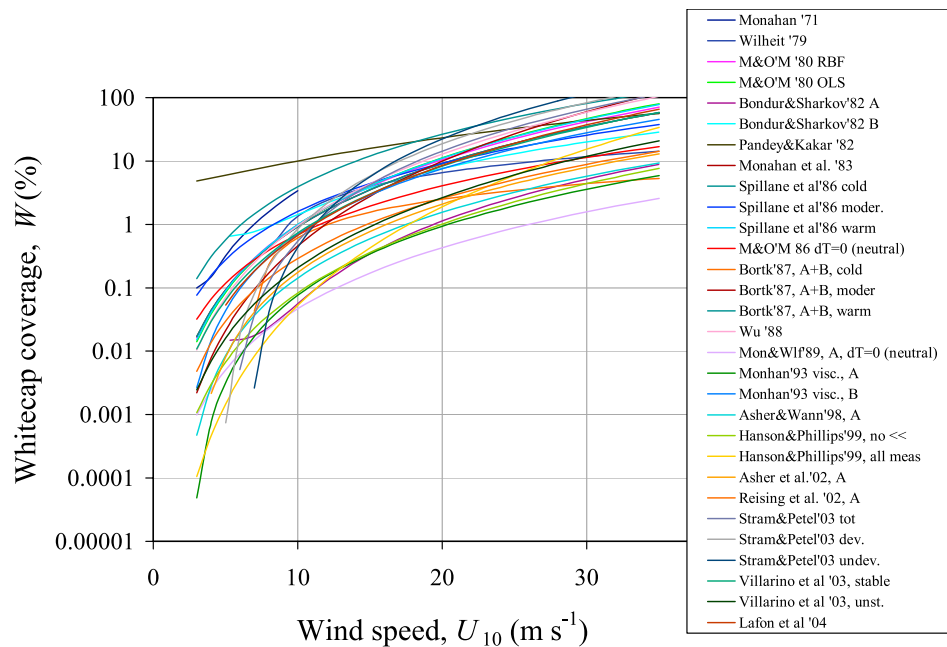


Figure 1. Various parameterizations for $W(U_{10})$ relation.

of wind speed alone cannot predict W well under various conditions encountered over the globe.

2.2. Factors Affecting Whitecap Coverage

[11] At different locations in the world ocean various environmental and meteorological factors act in concert but with different strengths and form a composite effect that either enhances or suppresses the effect of wind alone. Air-to-water energy input, sea state, and bubble lifetime are the physical quantities controlling the formation and spatial and temporal extent of whitecaps. Thus the variables that influence these quantities will influence whitecap coverage as well. Wind speed, U , atmospheric stability (the difference between seawater and air temperatures), ΔT , and surface current velocity, U_c , are variables necessary to completely describe the air-to-water energy flux and wind stress responsible for whitecap formation. Surface current velocity, U_c , wind fetch, X , duration of wind, d , sea surface temperature (SST), T_s , and concentration and type of surface active materials, C , affect sea state characteristics such as significant wave height, wave spectrum, wave dissipation rate, and wave age, and with that wave growth rate and the frequency of wave breaking. Thus these too affect whitecap formation and also determine the spatial extent of whitecap coverage. Finally, T_s , C , and salinity, S , affect water viscosity and surface tension. These, in turn, control (1) bubble formation and bursting by determining bubble size distributions when waves break and push air into the water, (2) bubble rise velocities through the water column to the surface, and (3) rates of coalescence and gravitational draining of bubbles floating on the surface. As a result, spatial extent and lifetime of whitecaps differ over the world ocean. Overall, besides wind speed, a suite of additional factors affect whitecap coverage, namely atmospheric stability, surface currents, wind fetch, wind duration, SST,

salinity, and surfactant concentration, $W(U, \Delta T, U_c, X, d, T_s, S, C)$.

[12] How different environmental and meteorological factors affect whitecap coverage can be summarized as follows [Monahan and O'Muircheartaigh, 1986; Stramska and Petelski, 2003]: Even low winds, around 3 m s^{-1} , may create whitecaps under unstable atmospheric conditions ($\Delta T > 0$), while moderate winds of 6 m s^{-1} may not lead to whitecapping when the lower atmosphere is stable ($\Delta T < 0$). Longer d produces a fully developed sea, which enhances W . In contrast, even high winds may produce fewer whitecaps if they blow for a short time. Fewer whitecaps form in places with limited X . Kraan *et al.* [1996] documented a decrease in whitecap coverage as the current velocity increased and suggested an explanation with an interaction of current shear and long waves. With T_s increasing, water viscosity decreases, which facilitates wave breaking and prolongs the lifetime of an individual whitecap. Both processes increase W . Organic compounds, such as amino acids, lipids, fatty acids, proteins, and phenols released into seawater from living organisms [Pinet, 1992, p. 128], create a surface-active film on the open ocean surface which damps capillary and short gravity waves [Hühnerfuss *et al.*, 1987; Alpers and Hühnerfuss, 1989]. This process slows down, or even prevents, the breaking process [Scott, 1986] yielding a decrease in W . Surfactants and salinity, S , lower the surface tension of seawater [Garrett, 1967; Scott, 1975] compared to that of fresh water. Systems with low surface tension require less work to create a new interface [Rosen, 1978]. Thus the air entrained from breaking waves in salt water ruptures into more and smaller bubbles compared to bubbles formed in fresh water [Cartmill and Su, 1993; Anguelova, 1997]. Surfactants quickly adsorb to the bubble walls stabilizing them against dissolution in the water column and inhibiting their coalescence and drainage

at the ocean surface [Garrett, 1967; Rosen, 1978; Thorpe, 1982; Blanchard, 1983; Scott, 1986]. This results in more persistent and long-lived whitecaps in seawater than in fresh water [Monahan and Zietlow, 1969]. Small variations of S in the open ocean may cause only small variations in W , but large S differences, such as between open ocean and coastal zones, could invoke more significant changes in W .

2.3. Modeling the Variability of Whitecap Coverage

[13] The understanding that various physical, chemical and biological factors influence whitecap formation and coverage has been around since Williams [1969] first suggested their possible effects on the $W(U_{10})$ relation. Since the first field campaigns [Monahan, 1971; Nordberg et al., 1971; Ross and Cardone, 1974], measured whitecap coverage has been reported together with wind speed and additional variables such as surface water and air temperatures and wind fetch. Quantifications of the effects of some of these additional factors have been published.

[14] The usual approach when considering the effect of water temperature on whitecap coverage has been to divide the range of observed T_s values into subranges of cold, moderate, and warm waters. In each T_s subrange different exponents [e.g., Spillane et al., 1986] or even functional expressions [e.g., Bortkovskii, 1987, Table 2.1] are chosen for the wind speed dependence. With a similar approach, Stramska and Petelski [2003] account for the wind duration effect by offering $W(U_{10})$ relations for developed and undeveloped seas assuming that during their experiment wind duration, not fetch, was the variable determining the sea state. Monahan and O'Muircheartaigh [1986, equation 5] proposed the first explicit relation quantifying the effect of an additional variable, that of atmospheric stability, $W(U_{10}, \Delta T)$. Expressions for $W(U_{10}, X)$ or $W(X)$ in fetch-limited conditions have been only recently proposed [Xu et al., 2000; Zhao and Toba, 2001; Piazzola et al., 2002; Lafon et al., 2004]. The dependence of whitecap coverage on the remaining factors (U_c , S , and C) is only qualitatively discussed.

[15] Another approach to address the necessity to account for additional factors has been the parameterization of W with one parameter or a combination of parameters, which accounts for the action of several variables that affect wave breaking and whitecapping. Proponents of W parameterization in terms of u_* or wind stress, τ , instead of U_{10} [Wu, 1979, 1988; Toba and Koga, 1986], have always had a strong point. Indeed, u_* obtained with Monin-Obukhov similarity theory using diabatic profiles [Liu et al., 1979; Large and Pond, 1981; Fairall et al., 1996] can explicitly account for ΔT and U_c . Also, the roughness length, z_0 , with terms for smooth and rough flows [e.g., Smith, 1988b; Fairall et al., 1996, equation 25] can implicitly account for the factors affecting the wavefield, namely U_c , X , d , and possibly T_s and C . However, even rigorously estimated u_* fails to remove the significant scatter of data in plots of $W(u_*)$. Compare, for instance, Figures 4 and 5 of Stramska and Petelski [2003] or Figures 2 and 3 of Lafon et al. [2004]. A large body of recent publications argues that wavefield characteristics must be explicitly included in z_0 for better results [Donelan et al., 1993; Fairall et al., 2000; Taylor and Yelland, 2001; Bourassa, 2004]. This argument is further supported by parameterizations of W in terms of

wave spectrum [Ross and Cardone, 1974; Snyder and Kennedy, 1983], wave age [Kraan et al., 1996], wave dissipation rate [Hanson and Phillips, 1999], and the breaking wave parameter (a dimensionless parameter combining u_* and wave spectrum) [Zhao and Toba, 2001], all of which demonstrate the strong correlation of W with wavefield characteristics. However, none of them alone suffice to completely describe W variability for, while all these parameterizations would account for energy input and to some extent for wavefield, they do not explicitly address the variables responsible for the whitecap lifetime, T_s , C , and S .

[16] In summary, the existing knowledge of whitecap coverage helps to identify and qualitatively understand the action of the additional factors affecting W . The effects of some of these factors have been quantified either explicitly, e.g., $W(\Delta T)$ and $W(X)$, or implicitly, e.g., $W(u_*)$. However, quantification of the effects of all additional factors in the form $W(U, \Delta T, U_c, X, d, T_s, S, C)$, admittedly cumbersome, or $W(u_*, T_s, S)$, is missing. To extract physically sound model(s) for the effects of these additional factors, a database of whitecap coverage under various environmental and meteorological conditions accompanied with simultaneous measurement of variables describing these conditions is necessary. Do existing measurements of whitecap coverage provide enough data to compile such a database?

2.4. Whitecap Coverage Measurements

[17] Traditionally, whitecap coverage is determined from still photographs or video images of the sea state collected from research platforms, ships, and aircraft. Facts for 28 data sets of W are summarized in Table 2 (we do not claim that this list of data sets is exhaustive). Figure 2 shows the locations of measurements. Though useful for gaining knowledge on whitecap coverage, the existing data sets do not provide enough information to model its high variability. A database for W built from the existing photographic measurements (here and onward under "photographic measurements" we mean both photographic and video measurements) of whitecap coverage would have the following weak points.

[18] First, Figure 2 reveals the patchiness of the conditions represented. Most of the data are collected in cold waters; only 5 data sets (156 total data points) represent warm water conditions ($T_s > 17^\circ\text{C}$), see Table 2. With the exception of data sets 10, 13, and to some extent 25, all data have been collected in coastal zones or in confined fetch-restricted seas. Also, only one data set is reported for the Southern Ocean. Overall, experiments conducted over a time span of 42 years have provided 853 data points (not including Mediterranean Sea data reported by Villarino et al. [2003]). No measurements are available for vast areas of the ocean, especially in the Southern Hemisphere. Thus existing data sets largely under represent open ocean conditions and areas with long fetches and persistent winds.

[19] Another issue with the photographic database is that there is not sufficient documentation of the meteorological and environmental conditions accompanying the whitecap coverage measurements. The conditions encountered during various experiments cover a wind speed range of 0.1–25 m s^{-1} (Figure 3a), an atmospheric stability range from -8 to $+12^\circ\text{C}$, and water temperatures from -1.7 to 30.55°C (Figure 3b). While the wind speed and stability

Table 2. Data Sets of Whitecap Coverage Observations^a

Data Set Number	Data Set	Data Points	Relative Error, %	Location	Time	Method	U_{10} Range, $m s^{-1}$	T_s , °C	Add. param. ΔT , S , X , d , C , U_c	Reference
1	US Squadron	5	NA	Caribbean area	Jun-Oct 1952	Aerial photos	4–20.6	NA	NA	Blanchard [1963, p. 160]
2		4	15	North Sea, North Atlantic	Mar 1969	Aerial photos	13–25	2–9 Tabulated	ΔT tabulated	Nordberg et al. [1971]
3	BOMEX	38	7–91	Barbados, Atlantic Ocean	May 1969	Photos	2.9–9	28–28.65	X tabulated	Monahan [1971], part of his Table 1
4		16	7–100	West Atlantic Coast	Jul-Aug 1969	Photos	0.1–17.7	17.4–30.55	ΔT tabulated	Monahan [1971], part of his Table 1
5		13	21–168	North Sea, Atlantic	Mar 1969	Aerial photos	9.7–23.3	NA	ΔT tabulated	Ross and Cardone [1974]
6		20	NA	Caribbean Sea	Jan 1971	Photos	10	NA	ΔT tabulated	Snyder et al. [1983] complete whitecap statistics
7		29	NA	Bight of Abaco, Bahamas Bank	1972?	Photos	8.5–18.8	24.7 Mean value	NA	Toba and Chien [1973]
8		6	NA	East China Sea	1972?	Photos	5–14	14.8–6 Range	NA	Kondo et al. [1973]
9		6	NA	Observation Tower Hiratsuka, Japan	1975–1978	Aerial photos	15–25	NA	NA	Bortkovskii [1987] (5 in his Figure 2.5)
10	Typhoon-75	39	22	western tropical Pacific	1975–1978	Photos	5–15	27–29 Range	X , C qualitatively	Bortkovskii [1987] (1 in his Figure 2.5)
11	Typhoon-78	64	13–396	NE Atlantic	Aug-Sep 1978	Photos	2.5–15.3	12.5–14 Tabulated	ΔT tabulated	Monahan et al. [1983b]
12	STREX	84	13–200	Gulf of Alaska	Nov-Dec 1980	Photos	2.7–17.2	5.11–11.11 Tabulated	ΔT tabulated	Doyle [1984]
13	RV-Bugaev	34	40	North Atlantic Kuroshio	1979–1980	Photos	9–24	3–15, 10–23 Ranges	X , C qualitatively	Bortkovskii [1987] (2 in his Figure 2.5)
14		6	71–126	Black and Barents seas	1981?	Aerial photos	4.7–10.5	12 Mean value	NA	Bondur and Sharkov [1982]
15	POLEX-YUG	31	40	Seas Scotia, Weddell, Bellingshausen	Dec 1981	Photos	8.5–18	–1.7 to +3 Range	X , C qualitatively	Bortkovskii [1987] (3 in his Figure 2.5)
16	MIZEX83	32	6–200	North Atlantic Arctic Ocean	Jun-Jul 1983	Photos	4.7–14	–1.3 to 14.4 Tabulated	ΔT tabulated	Monahan et al. [1984]
17	MIZEX84	102	14–650	North Atlantic Arctic Ocean	Jun-Jul 1984	Photos	2.6–16.4	–1.17 to 9.9 Tabulated	ΔT tabulated	Monahan et al. [1985]
18		32	NA	North Atlantic George Bank	April 1990	Video images	1–17	5.5 Mean value	NA	Asher and Wanninkhof [1998], A stage
19	SS&ASI Exp Critical Sea test Program	65	NA	Gulf of Alaska	Feb-Mar, 1992	Video images	5–15	NA	NA	Hanson and Phillips [1999]
20	ASGASEX	44	5–10	Meestpost Noordwijk, Dutch coast	1993	Photos	NA	NA	NA	Kraan et al. [1996] A stage
21		9		Bohai Bay, China	Oct-Nov, 1995	Photos	3–20	15–17	ΔT range	Xu et al. [2000]
22	FETCH	45		Gulf of Lion Mediterranean	Mar-Apr 1998	Photos	6–17	13	$\Delta T = [-2.65 \text{ to } 6.25]$	Lafon et al. [2004]
23	GASEX98	62	NA	North Atlantic	May-Jun 1998	Video images	5–16	NA	NA	Asher et al. [2002], A stage; ΔT , T_s
24	SHOWEX	NA	NA	Outer Banks, NC, USA, Atlantic ocean	Nov-Dec 1999	Video images	7.2, 9.8, 13.6	NA	X	S obtainable from authors Melville and Matusov [2002]
25	FAIRS	4	NA	Northeastern Pacific Ocean	Sep-Oct 2000	Video images	2–15	16.3 Mean value	NA	Reising et al. [2002]
26		63	NA	North Atlantic	Jun-Aug 1998	Photos	5–13	2–13 Range	X order	Srammska and Petelski [2003]
27	WISE 2000	20,000	NA	Mediterranean sea	Nov-Dec, 2000	Video images	<3–15	17.5–14	$\Delta T \approx 2$ °C;	Villarino et al. [2003] and Camps et al. [2002]
28	WISE 2001	63,000	NA	Mediterranean Sea	Jan 2001	Video images	10–25	22–16	$S = 38$ psu	Villarino et al. [2003] and Camps et al. [2004]
					Oct-Nov 2000	Video images			$\Delta T = -2$ to -12 °C;	
									$S = 38$ psu	

^aListed chronologically according to the time of the field campaign (time column).

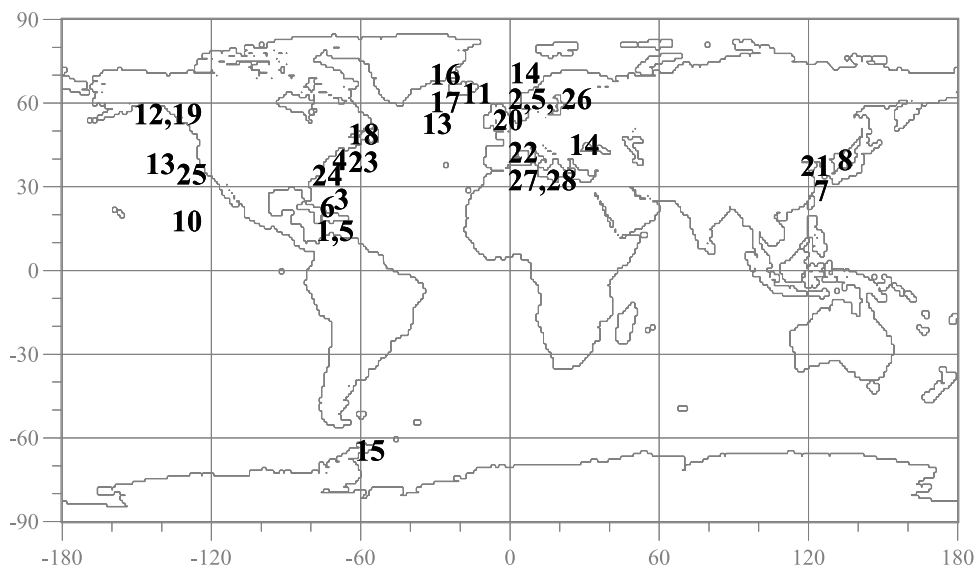


Figure 2. Locations of photographic measurements of whitecap coverage.

conditions are well represented and ensure an empirical derivation of $W(U_{10})$ and $W(\Delta T)$, the T_s range is presented in discrete intervals and cannot be used to extract well constrained relations for $W(T_s)$. Only two of the listed data sets (27 and 28) report accompanying measurements of S . Five data sets report tabulated values for fetch. Only Kraan *et al.* [1996] report concomitant data for U_c . Wind duration and presence of surfactants are not reported quantitatively.

[20] Third, while processing photographs or video images to extract whitecap coverage, an intensity threshold needs to be chosen to separate whitecaps from surrounding water. Asher and Wanninkhof [1998] and Stramska and Petelski [2003], among others, describe well the typical steps of analyzing photographs and/or video images of whitecaps. The choice of this threshold is always somewhat subjective, and can vary from data set to data set leading to large uncertainties in the whitecap coverage estimates [Blanchard, 1963; Nordberg *et al.*, 1971; Ross and Cardone, 1974; Bondur and Sharkov, 1982; Kraan *et al.*, 1996].

[21] Finally, photographs and video images register well the more visible active whitecaps, stage A in Monahan and Woolf's [1989] terminology, while aged whitecaps (stage B), which are thinner and less bright, can be easily overlooked. Since aged whitecaps cover much larger areas than freshly generated active whitecaps [Monahan, 1989], measuring whitecap coverage from photographs and video images tends to underestimate W , especially at low and moderate winds. Moreover, the oblique angle of observation in the photographs and video images prevents detection of the B stage of the whitecaps and introduces additional underestimation; see for example area 2 in Figure 2 of Stramska and Petelski [2003].

[22] In summary, the existing measurements of whitecap coverage, though of high quality, are not sufficient to quantify the dependence of W on other environmental and meteorological variables in addition to wind speed. Therefore, to model the high variability of whitecaps, a database

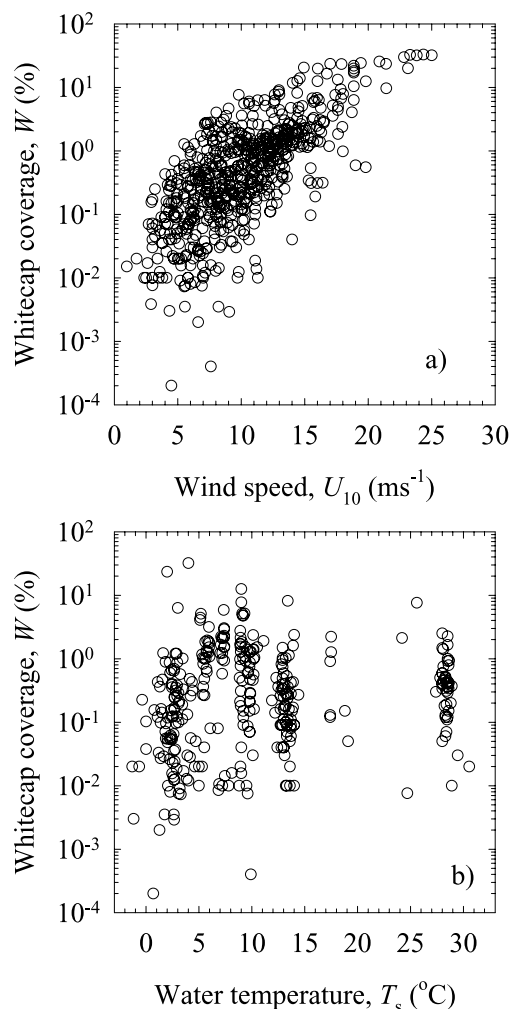


Figure 3. Major dependencies from photographic measurements of whitecap coverage: (a) $W(U_{10})$ and (b) $W(T_s)$.

of W over the entire globe is needed, and this requires an alternative approach for estimating whitecap coverage. Can we use satellite measurements?

2.5. Remote Sensing Signature of Whitecaps

[23] Being a mixture of air and water, both foamy whitecaps on and bubbly clouds below the surface have dielectric properties very different from those of seawater and this determines their specific signature for remote sensors. Whitecaps can be detected from space-borne remote sensors in various portions of the electromagnetic spectrum. They appear as high reflectivity in the visible or high emissivity in the microwave or a combination of reflectivity and emissivity signals in the IR [Whitlock *et al.*, 1982; Koepke, 1984, 1986; Frouin *et al.*, 1996; Kokhanovsky, 2004; Marmorino and Smith, 2005]. Any of these signals can be used for detection of whitecaps. The preferred choice, however, is the microwave region (frequency of 1 GHz to 3 THz or wavelength of 10 to 0.01 cm) because atmospheric interference is a more manageable problem compared to visible and IR wavelengths [Gordon and Wang, 1994; Swift, 1990]. The variable measured at microwave frequencies and suitable for whitecap coverage detection is brightness temperature, T_B , which is connected with the emissivity, e , of foam-covered ocean through the physical temperature, T_s , of the seawater: $T_B = eT_s$.

[24] At microwave frequencies, the radiation available for remote sensing emanates from a thin layer (penetration depth) at the surface. Depending on the wavelength and the dielectric properties of the sensed media (water or foam), this penetration depth differs. For seawater it is from less than a millimeter at 37 GHz to a few centimeters at 6 GHz. For foam with different content of air and water the penetration depth varies over a wider range. Thus passive microwave sensors detect the surface part of the whitecaps, that is, the floating bubble rafts at the surface, not the bubble plumes below. At lower frequencies, however, bubble plumes below thin foam patches can be sensed.

[25] The use of microwave frequencies to diminish atmospheric interference raises, however, the question of losing resolution. Indeed, none of the current satellite-borne microwave sensors, even with the smallest antenna footprint of 4 km \times 6 km (AMSR-E, 89 GHz [Kawanishi *et al.*, 2003]), can resolve an individual whitecap having a length scale of at most 10 m [Bortkovskii, 1987; Dahl and Jessup, 1995]. Whitecap coverage detection, however, does not require resolving and counting individual whitecaps. Rather, what is of interest is how much the average emission of a given ocean area changes with whitecaps appearance and how well these changes can be retrieved from measured data.

3. Method Estimating Whitecap Coverage

3.1. Physical Concept

[26] The concept of estimating whitecap coverage on a global scale from satellite data relies on changes of ocean surface emission at microwave frequencies induced by the presence of whitecaps. Ocean surface emissivity, e , is a composite of two main contributions: emissivity due to the rough sea surface, e_r , in places free of whitecaps ($1 - W$),

and emissivity due to foam, e_f , in places covered with whitecaps W . The composite surface emissivity therefore can be presented as [Stogryn, 1972]

$$e = e_r(1 - W) + e_f W. \quad (1)$$

Provided that the emissivities in (1) can be obtained, whitecap coverage can be determined as

$$W = \frac{e - e_r}{e_f - e_r}. \quad (2)$$

In (2), e can be retrieved from satellite measurements with appropriate atmospheric correction, while emissivities e_r and e_f can be computed using analytical or empirical models. Since e obtained for each point on the globe is a measure of ocean emissivity as it is created by the specific environmental and meteorological factors at this point, the satellite-measured W values will contain information for the additional factors and be more realistic than W predictions from a model developed from regional data elsewhere.

[27] The surface emissivity model (1) appears deceptively simple. There are two major requirements for the applicability of (1), which are difficult to fulfill. First, the models for e_r and e_f must clearly separate these two emissivities: e_r must represent rough sea emission not contaminated by foam emission and e_f must strictly represent emissivity of foam. While even simple foam emissivity models can guarantee the latter, existing models for rough surface emission most certainly contain foam contributions making the former the more challenging task. Second, only well validated models for e_r , e_f , and the atmospheric correction of e can guarantee the true utility of (1). However, the existing uncertainty in validation of atmospheric terms, the continuous development of rough surface models, and the insufficient knowledge of foam emission all demand tuning of some parameters in or applying empirical corrections to those models. Moreover, the lack of whitecap coverage values representing a wide range of conditions impedes reliable constraints on such tuning and empirical corrections.

[28] However challenging, these difficulties are by no means prohibitive. In fact, the idea of using a surface emissivity model (1) in combination with satellite data to obtain whitecap coverage is not completely new and has been tried before. In developing forward models of ocean microwave emission for geophysical retrieval algorithms in the early 80s, the remote-sensing community has used (1) and measurements of T_B from the Scanning Multichannel Microwave Radiometer (SMMR) to infer foam coverage [Pandey and Kakar, 1982; Wentz, 1983]. The need to measure whitecap coverage on a global scale and model its high variability more realistically clearly calls for a renewed effort aimed at assessing the feasibility of obtaining W from routine satellite measurements.

[29] In the following sections, using current better calibrated satellite data, we demonstrate the feasibility of the concept and present the first global estimates of satellite-based whitecap coverage. In this endeavor we do not seek the most rigorous models for computing the emissivities in (2). Rather we use readily available models and empirical parameterizations and accept simplifying assumptions that

would allow the implementation to advance to a reasonable end.

3.2. Analytical Expressions

3.2.1. Surface Emissivity e

[30] The composite surface emissivity, e , can be retrieved from satellite-measured brightness temperature, T_B , of the ocean surface. T_B , registered by a microwave radiometer viewing the ocean from a satellite, is given by the radiative transfer equation [Stewart, 1985; Swift, 1990]:

$$T_B = eT_s + T_{BU} + (1 - e)tT_{BD} + (1 - e)t^2T_{CB}. \quad (3)$$

Here only the first term, which gives the ocean surface emission influenced by the atmospheric transmission, t , carries information regarding W . The remaining three terms represent the contribution of the atmosphere, namely upwelling and downwelling atmospheric radiation, T_{BU} and T_{BD} , and cosmic background radiation T_{CB} . The factors $1 - e = r$, t , and t^2 account for the radiation reflected from the ocean surface back to space and its attenuation on the way up and down through the atmosphere. We neglect the so-called omega term [Wentz, 1997], which accounts for nonspecularly reflected downwelling radiation. Solving (3) for e yields the emission from the ocean surface only:

$$e = \frac{T_B - T_{BU} - tT_{BD} - t^2T_{CB}}{tT_s - tT_{BD} - t^2T_{CB}}. \quad (4)$$

All quantities in (4) may be either measured or analytically evaluated. Satellite-borne sensors provide daily measurements of T_B and T_s . Wentz [1997] derived approximate formulae for the atmospheric terms T_{BU} and T_{BD} as a function of columnar water vapor, V [mm], and cloud liquid water, L [mm]. Both of these are derived as geophysical products from measured T_B . The cosmic background is known, $T_{CB} = 2.725$ K [Smoot and Scott, 2000]. The atmospheric transmittance, t , at microwave frequencies involves four major components due to rain, cloud liquid water, molecular oxygen, and water vapor [Wilheit et al., 1980; Swift, 1990; Wentz, 1997]. Correction for rain is a complex problem, thus we model the transmittance of the nonraining atmosphere. The transmittance for a one-layer atmosphere along a viewing path is approximated with [Wentz, 1997]

$$t = e^{-k \sec \theta} \quad (5a)$$

$$k = a_O + a_V + a_L, \quad (5b)$$

where θ is the incidence angle of the sensor (the angle measured from the normal to the probing beam), and k is attenuation coefficient accounting for the effects of oxygen with absorption coefficient a_O , of water vapor with a_V , and of cloud liquid water with a_L . Wentz [1997, equations 20–23] gives expressions for each of these absorption coefficients as a function of V , L , and T_s .

3.2.2. Rough Sea Emissivity e_r

[31] Over foam-free areas of the ocean surface at low to moderate wind speeds (< 10 m s⁻¹), surface roughness is the major contributor to changes of ocean surface emission and

Table 3. Regression Coefficients in (7)^a

Coefficient	Value
h_0	0.115
h_1	3.8×10^{-5}
v_0	0.117
v_1	-2.09×10^{-3}
v_2	7.32×10^{-2}

^aSee Pandey and Kakar [1982].

consequent changes of brightness temperature [Stogryn, 1972; Swift, 1990]. To model the emission of a rough sea, we have adopted the approach of Pandey and Kakar [1982]. The emissivity of rough sea surface, e_r , is considered as $e_r = e_s + \Delta e_r$, where e_s is specular emissivity of a flat ocean surface, and Δe_r accounts for changes of e_s due to wind induced surface roughness.

[32] Specular emissivity is obtained as $e_s = 1 - r_s$, where r_s is specular reflectivity calculated with the Fresnel formula [e.g., Swift, 1990, equations 6 and 7]. The calculation of r_s requires the dielectric constant of seawater, ϵ , usually modeled with the Debye equation [Rosenkranz and Staelin, 1972]. The dielectric constant of seawater is a complex number, $\epsilon = \epsilon' - i\epsilon''$, whose real component, ϵ' , represents the actual magnitude of the dielectric constant and the imaginary part, ϵ'' , is a measure of the attenuation (losses) of incident radiation in the material:

$$\begin{aligned} \epsilon' &= \epsilon_\infty + \frac{\epsilon_s - \epsilon_\infty}{1 + \omega^2\tau^2} \\ \epsilon'' &= \frac{\omega\tau(\epsilon_s - \epsilon_\infty)}{1 + \omega^2\tau^2} + \frac{\sigma}{\omega\epsilon_0} \end{aligned} \quad (6)$$

Here $\omega = 2\pi f_r$ is the frequency of the radiation (in radians) interacting with the material, f_r is the frequency in Hz, ϵ_∞ is the dielectric constant at infinite frequency, ϵ_s is the static dielectric constant, τ is the relaxation time, σ is the ionic conductivity of water, and ϵ_0 is the permittivity of free space. Klein and Swift [1977, equations 13–18] proposed empirical expressions for the static dielectric constant, $\epsilon_s(T_s, S)$, and relaxation time, $\tau(T_s, S)$, as functions of seawater temperature, T_s , and salinity, S . Values for ϵ_∞ , ϵ_0 , and σ are available from the literature [Hasted, 1973; Stewart, 1985]; f_r , thus ω , is chosen (section 3.3.1).

[33] We model the surface roughness correction, Δe_r , for both horizontal and vertical polarizations, with empirical expressions cited by Pandey and Kakar [1982], but do not use the constant bias that they introduce

$$\begin{aligned} \Delta e_{rh} &= \frac{U_{10}}{T_s} (h_0 + h_1\theta^2) \sqrt{f_r} \\ \Delta e_{rv} &= \frac{U_{10}}{T_s} (v_0 + v_1e^{v_2\theta}) \sqrt{f_r} \end{aligned} \quad (7)$$

Here h_i and v_i are coefficients (Table 3). U_{10} values are derived as a geophysical product from SSM/I-measured T_B analogously to V and L . The rationale of choosing these simple empirical expressions is that they are developed using Hollinger's [1971] data for which the effect of foam has been excluded, thus providing a clear separation between the contributions of roughness and foam in (1) and (2).

3.2.3. Foam Emissivity e_f

[34] Foam emissivity is obtained as $e_f = 1 - r_f$, where r_f is foam reflectivity calculated with the Fresnel formula. The dielectric constant of foam is determined as [Troitsky, 1962; Droppleman, 1970; Wentz, 1974]

$$\epsilon_f = \epsilon \frac{2Q\epsilon - 2Q + 3}{3\epsilon - Q\epsilon + Q}, \quad (8)$$

where Q is the ratio of the amount of water to total amount of air-water mixture within a unit volume. A more informative quantity for foam is the void fraction, α , defined as the ratio of the amount of air to the total amount of air-water mixture in a unit volume; the higher the void fraction, the more air the foam contains. Both these quantities are simply related as $\alpha = 1 - Q$.

[35] For the calculations of foam dielectric constant, we choose a void fraction $\alpha = 98\%$ ($Q = 2\%$). This choice is not arbitrary. This value is chosen to account for two main characteristics of microwave emission from sea foam: (1) high, black-body-like emissivity [Williams, 1969; Rose et al., 2002] and (2) a decrease of emissivity as foam thickness decreases [Droppleman, 1970]. According to Droppleman's [1970] model, with the choice of 98% void fraction, the computed ϵ_f and e_f represent all whitecaps thicker than 6 mm. Thinner foam layers will be missed and this may introduce some underestimation of W . This underestimation, however, is compensated for by our assumption of a foam layer with constant void fraction instead of a gradual change from $\approx 100\%$ at the surface to $\ll 1\%$ within the bubble clouds. Understanding the possible underestimation and overestimation of W with a choice of a constant void fraction of 98%, we believe that, compared to photographic measurements, this method evaluates more adequately the whitecap coverage because it "feels" both the thick active whitecaps in their initial A stage, and, though not all, most of the B stage of decaying whitecaps.

[36] Though our approach for calculating foam emissivity e_f differs from existing empirical and analytical models [Ulaby et al., 1986, chap. 18], it is suitable for the purpose of proof of feasibility. Indeed, it oversimplifies the foam emission problem considered rigorously in analytical models [Droppleman, 1970; Raiter and Sharkov, 1982; Chen et al., 2003], yet it has a stronger physical foundation than the empirical models [e.g., Stogryn, 1972] because it introduces the necessary dependencies of e_f on θ and f_r via r_f and also involves the specific features of foam as a medium via ϵ_f .

3.3. Data

[37] Computations of the emissivities in (2) require data for brightness temperature, T_B , water vapor, V , cloud liquid water, L , wind speed, U_{10} , SST, T_s , and salinity, S .

3.3.1. SSM/I Data for T_B , U_{10} , V , and L

[38] Special Sensor Microwave Imager (SSM/I) provides T_B , U_{10} , V , and L daily on a global scale. SSM/I is a passive microwave sensor, which detects natural microwave emission from the Earth's surface and atmosphere at four frequencies (19.35, 22.2., 37.0, 85.5 GHz) and horizontal (h) and vertical (v) polarizations [Hollinger et al., 1990; Wentz, 1997]. Brightness temperature T_B in the range from 100 to 300 K is the basic information the SSM/I collects. Values for U_{10} , V , and L are derived as geophysical products from T_B .

[39] The Global Hydrology Resource Center (GHRC) at Marshall Space Flight Center (MSFC), NASA, distributes T_B , U_{10} , V , and L data processed with Wentz's [1992] algorithm in full (swath) and reduced (gridded) resolution in hierarchical data format (HDF) files (<http://ghrc.msfc.nasa.gov>). Data used in this work are in arrays of 720×360 elements representing Earth's surface in $0.5^\circ \times 0.5^\circ$ gridded maps (54 km \times 54 km at the Equator). While the T_B values are not corrected for atmospheric effect, the U_{10} values are for the ocean surface. Valid U_{10} values range from 0 to 40 m s⁻¹, V values are in the range of 0 to 10 g cm⁻², and L values are from 0 to 1000 mg cm⁻². For the computations, the units of V [g cm⁻²] and L [mg cm⁻²] are converted to [mm] using the relation 1 g m⁻² $\times 10^{-3}$ = 1 mm [Wentz, 1997].

[40] For the estimation of W we choose to use 19.35 GHz, h polarization, for the following reasons. First, changes in ocean surface emissivity should be predominantly due to surface roughness and presence of foam, and not to other factors at the chosen frequency. Ocean emissivity changes not only with surface roughness and the presence of sea foam, but also with salinity, S , and seawater temperature, T_s . Salinity influences ocean emission weakly for frequencies from 5 to 50 GHz, and contributes more strongly for frequencies below 5 GHz [Wilheit, 1978]. At an incidence angle of 55° over the range of 0° – 30° C, brightness temperature of the ocean surface, T_B , is independent of T_s (i.e., $\partial T_B / \partial T_s \cong 0$) only for two frequencies: around 1.5 GHz and 27 GHz [Wilheit, 1978, Figure 5]. Considering the strong effect of S at low frequencies, the only suitable choice fulfilling the first requirement for the SSM/I incidence angle of 53.4° is around 23 GHz. Second, at the chosen frequency, the atmospheric effects need to be as little as possible. For SSM/I frequencies this requirement is fulfilled for 19 and 37-GHz channels. Combining these possible choices with the outcome of the first requirement singles out 19 GHz as the more suitable frequency. The choice of h polarization is based on results of radiometric experiments showing that the h polarization of T_B has higher sensitivity to changes in surface wind speed, and hence to formation of whitecaps [Hollinger, 1971; Webster et al., 1976; Wilheit, 1978; Pandey and Kakar, 1982; Wang et al., 1995]. A 1-m s⁻¹ change of wind speed invokes a change of about 0.5 K in vertically polarized T_B while horizontally polarized T_B changes with about 1.2 K. The h polarization signal includes both surface roughness and foam effects, which, we believe, are well separated with our choice of model for roughness emissivity (section 3.2.2).

3.3.2. AVHRR T_s Data

[41] The advanced very high resolution radiometer (AVHRR) provides sea surface temperature, T_s , on a daily basis. AVHRR is a visible/infrared multispectral scanner, which registers the Earth/atmosphere radiation in five channels. The Physical Oceanography Distributed Active Archive Center (PODAAC) at the Jet Propulsion Laboratory (JPL), NASA, distributes global maps of SST data in several temporal and spatial resolutions in various formats including HDF (http://podaac.jpl.nasa.gov/sst/sst_data.html). For consistency with the resolution of the SSM/I data sets, T_s data gridded at $0.5^\circ \times 0.5^\circ$ resolution are used in this study. The SST values are obtained with the Pathfinder SST algorithm. The coefficients of the algorithm are calcu-

lated by regressing observations of satellite skin SST to buoy measurements of bulk SST thus computing “pseudo-bulk SST” values [Emery *et al.*, 2001]. Therefore the error introduced in the computation of emissivities (e_s , e_r , and e_f) from the difference between skin and bulk SST is not significant, especially at 19 GHz.

[42] We have used the so-called “best SST” product, which retains only pixels with the highest quality, discarding areas with clouds and areas from the far and distorted portion of the swath. As a result, there is not complete coverage within satellite passes. Because all other data sets used for the computations have more complete coverage, the daily T_s maps determine the cell number and locations for which all necessary data exist and match. Thus, from each T_s map, a mask containing pixels available for the computations is created for each day.

[43] The range of values used for the calculations is -1.8 to about 33°C . We discarded extremely low SST values (below -1.8°C) because they are most probably attributed to seawater mixed with ice (slush). Since the emission of sea ice is as high as that of whitecaps, their signals cannot be distinguished. Discarding $T_s < -1.8$ removes about 2% of all available T_s values.

3.3.3. WOA98 S Data

[44] The World Ocean Atlas 1998 (WOA98) provides global maps of seawater salinity, S , at 33 standard levels covering depths from 0 to 5500 m [Levitus *et al.*, 1998]. The WOA98 is based on the extensive World Ocean Database 1998 (WOD98) of the National Oceanographic Data Center (NODC), which contains more than 4 million in situ data entries measured with various instruments including historical oceanographic records, bottle seawater samples (ocean station data), and conductivity-temperature-depth (CTD) instruments. Data are offered as text files, which contain several “stacked” 10×6480 arrays, one for each depth level (http://www.nodc.noaa.gov/OC5/data_woa.html). We use $1^\circ \times 1^\circ$ maps of monthly climatological means of S at the surface, i.e., the first 10×6480 array in a file for a given month. This array is rearranged into 360×180 array to represent a $1^\circ \times 1^\circ$ map and then resampled via bilinear interpolation to obtain a $0.5^\circ \times 0.5^\circ$ map (720×360 array).

3.3.4. Data Preparation

[45] Data sets of T_B , V , L , U_{10} , and T_s for all 365 days and S for all 12 months of 1998 are used. Data are first processed to obtain consistency in the spatial resolution, validity of the values, unification of the units, and spatial and temporal matching. Next, wind, rain, and clear sky masks are prepared for each day and applied to all data.

[46] The wind mask is extracted from the daily U_{10} maps. The wind mask favors cells with wind speeds $\geq 3 \text{ m s}^{-1}$, the wind speed for whitecap inception, and discards cells (puts 0s) with lower wind. Very high winds, $U_{10} > 35 \text{ m s}^{-1}$ are also excluded since the SSM/I is not designed for high winds and its performance deteriorates under gale conditions. The wind mask removes about 2% of the pixels representing the ocean. An examination of data for the entirety of 1998 showed that wind speed is rarely above 26 m s^{-1} .

[47] Since the atmospheric transmittance obtained with (5) is for a nonraining atmosphere, a rain mask is necessary. A cell is considered rain-free when two requirements, formed from h and v polarizations of T_B

Table 4. Temperatures Used in Condition (9) for a Rain Mask^a

Zone	Latitude	T_0 , K	T_1 , K
Tropics	0° – 25°	50	175
Midlatitudes	25° – 55°	50	165
Arctic	55° – 90°	50	130

^aCompiled from Tables 1 and 4 of Goodberlet *et al.* [1989].

at 19 and 37 GHz, are fulfilled simultaneously [Goodberlet *et al.*, 1989]:

$$T_B(37\nu) - T_B(37h) > T_0$$

$$T_B(19h) < T_1, \quad (9)$$

where T_0 and T_1 have different values depending on the latitude (Table 4). The rain mask removes about 14% from the useful “ocean” pixels. Apparently most of the removed cells are associated with high T_s , which could introduce bias in the distribution of T_s values toward lower temperatures. Figure 4a displays the distributions of T_s for one day (27 March 1998) without (black bars) and with (white bars) the mask applied, and the percentage of removed cells for each temperature bin (gray circles and solid line with axis at right). Indeed, the rain mask removes more cells with T_s in the range of 25° – 33°C (about 34%) than with lower T_s values (15–25% for 5° – 25°C). However, it also removes many cells, around 30%, for the lowest SST. The shape of the masked distribution, however, does not change significantly compared to the initial distribution. There is not noticeable skewness toward lower T_s values. In addition, the averages of the initial (20.02°C) and masked (19.22°C) T_s values differ by only 4%. Thus, despite the apparently preferential removal of high and low T_s , the effect of the rain mask is still tolerable.

[48] The clear sky mask, prepared from daily L maps, discards cells with high cloud liquid water content leaving clear sky cells with $L \leq 5 \text{ mg cm}^{-2} = 0.05 \text{ mm}$ [Wentz *et al.*, 1980]. The expected adverse effect of this mask is the introduction of a bias toward lower wind speed values, thus missing locations with high whitecap coverage. Figure 4b shows the distributions of U_{10} for the same day (27 March) without (black bars) and with (white bars) the mask applied, and the percentage of removed cells for each wind speed bin (gray circles and solid line with axis at right). Only wind speed bins with more than 200 points are considered; for wind speeds above 22 m s^{-1} there are very few points in a bin, which compromises the statistics. Figure 4b demonstrates that the removal of wind speed values is roughly proportional to the amount of data in each bin leading to a decrease in the absolute number of cells available for retrieval of whitecap coverage, but not changing the shape of wind speed distribution. The average of the initial wind speed values is 10.53 m s^{-1} , while that of U_{10} values remaining after application of the mask is 10.5 m s^{-1} . Obtaining W under clear sky conditions, we decrease the uncertainties that would arise from the difficulties in parameterizing and validating cloud liquid water product, L , from radiometric measurements [Wentz, 1997]. Once the feasibility of satellite-based estimates of W is tested, the task of retrieving whitecap coverage under cloudy conditions can be pursued. The application of a clear sky mask removes up to 40% of the “ocean” pixels. For the remain-

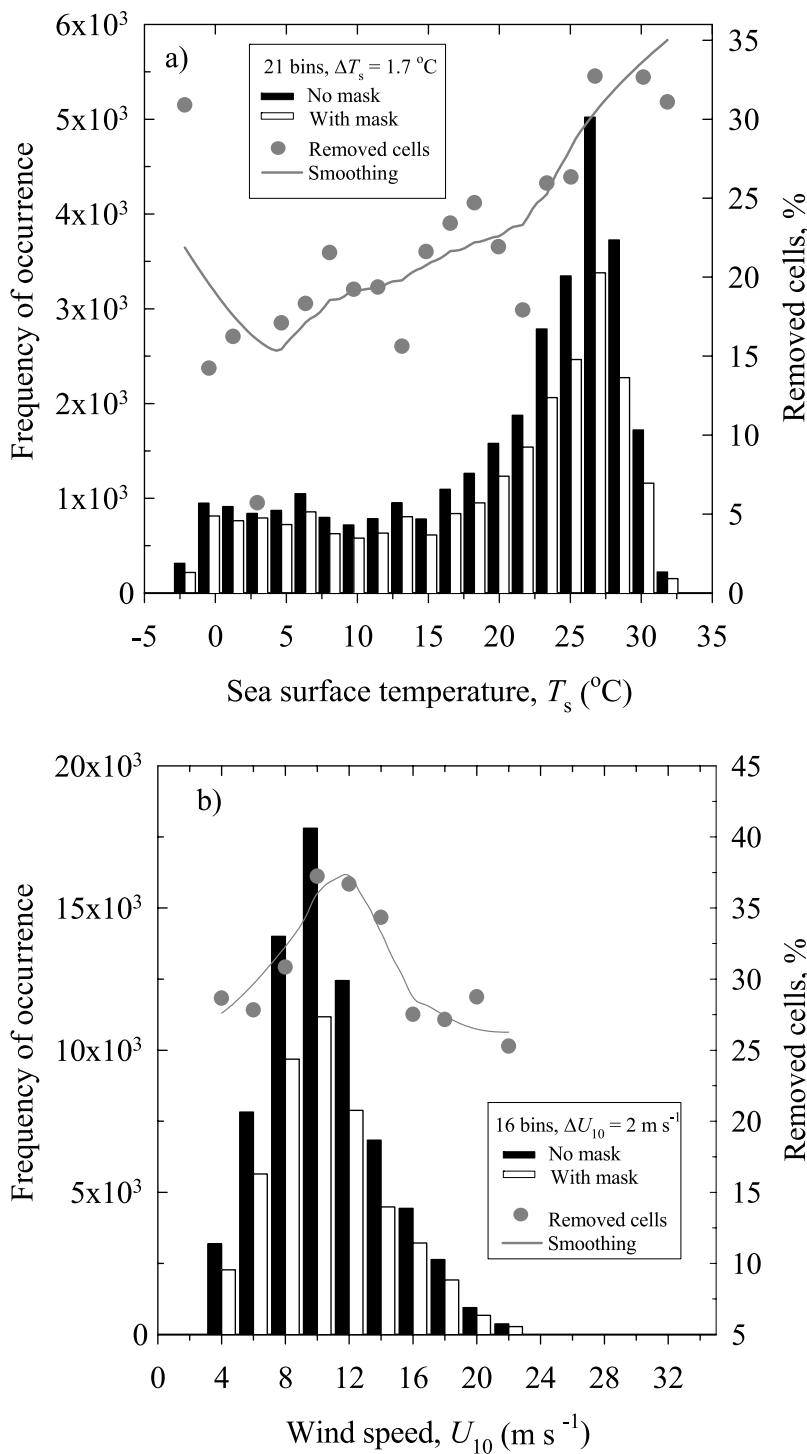


Figure 4. Changes in data distributions when masks are applied: (a) Effect of rain mask on the distribution of T_s values; (b) effect of cloud mask on the distribution of U_{10} values.

ing 60% of “ocean” pixels, we assume $L \cong 0$, thus $a_L \cong 0$. This yields a modified attenuation coefficient in (5b), $k = a_O + a_V$, where the absorption coefficients of oxygen and water vapor are determined with high confidence.

[49] These three masks for wind, rain, and clear sky, together with the mask matching SSM/I products with available T_s , combine to form one composite mask. This composite mask is applied to S , T_s , T_B , U_{10} , and V , and with that, all

necessary data sets are ready for the computation of the emissivities and W in (2). On that particular day of 27 March the composite mask removes about 83% of the initial ocean pixels for T_B , leaving about 15,800 cells available for W estimation. These numbers cited for 27 March 1998 vary from variable to variable (U_{10} , V , T_s , S) and from day to day, yet remain of the same order of magnitude. For all days of 1998, the number of pixels useful for W estimation ranges

from a minimum of about 6,700 in November to maximum of 27,000 in October. This constitutes 4% to 17% of all pixels representing the oceans on a $0.5^\circ \times 0.5^\circ$ global map.

3.4. Error Analysis

[50] The method for estimating global whitecap coverage, W , uses many measured and calculated quantities. Assuming that the models used (section 3.2) are exact, that is, there is no modeling error, the main source of error is the uncertainties in data measurements. These are carried over to the calculated variables and ultimately to the final result. To determine the uncertainty with which the method retrieves W , an analysis of the error propagation and the contributions of the various quantities to the error of W has been made using the approach outlined by *Bevington* [1969, chap. 4].

[51] The analysis of each investigated quantity starts with two considerations: (1) on which variables this quantity depends, and (2) which covariant terms are likely to play a role. The error analysis derives the variance of calculated W , σ_W^2 , as a function of the variances of the four emissivities and two covariant terms:

$$\sigma_W^2 \leq W_e \sigma_e^2 + W_s \sigma_{e_s}^2 + W_f \sigma_{e_f}^2 + W_r \sigma_{e_r}^2 + 2W_{er} \sigma_e \sigma_{e_r} + 2W_{sf} \sigma_{e_s} \sigma_{e_f} \quad (10)$$

where the sensitivity coefficients W_{ij} are calculated using the computed emissivities (Appendix A). The variance of each emissivity ($\sigma_{e_s}^2$, $\sigma_{e_r}^2$, $\sigma_{e_f}^2$ and $\sigma_{e_r}^2$) is derived as a function of the basic variables whose measurement errors influence them, namely T_B , V , U_{10} , T_s , S , ε_∞ , σ , θ , and Q , and whose errors propagate to the errors of the emissivities. For instance, composite sea emissivity emerges as a function of four basic variables, $e = f(T_B, T_s, V, \theta)$, while more variables affect foam emissivity, $e_f = f(T_s, S, \theta, \sigma, \varepsilon_\infty, Q)$. The variances of the four emissivities in (10) are listed in Appendix A. The variances and standard deviations of the basic variables are either known from their measurement and calculation or are chosen (Table A1).

4. Whitecap Coverage From Satellite Data

4.1. Results

[52] Having all necessary analytical and error expressions, initial values, and prepared data at hand, the calculation of the emissivities and whitecap coverage in (2) proceeds. On a global map for 27 March 1998, specular emissivity e_s remains relatively low and varies in a narrow range, from 0.255 to 0.285, conforming to the contention that in the microwave range a smooth flat ocean is a cold body with low emissivity. Emissivity due to roughness, Δe_r , ranges from 0.0095 to 0.0832, adding little but a measurable correction to e_s as the wind roughens the sea surface. As expected, foam emissivity, e_f , has high values, from 0.913 to 0.942. Finally, composite seawater emissivity, e , ranges from 0.25 to 0.45. With these values, the range of estimated whitecap coverage for 27 March 1998 is from less than 1% to about 24% with 97% of all estimated values in the range of 0.6% to 6%.

[53] Figure 5a shows the global spatial distribution of monthly mean whitecap coverage for March 1998. White-

cap coverage over most of the world ocean is up to 4%. The lowest whitecapping, from less than 1% up to 2%, is evident along the equator, on the western edges of the continents, and east of the tip of South America. The highest whitecapping, up to 6%, is observed in the zonal belts of the trade winds (5° to 30° N and S) and the prevailing westerlies (30° to 60° N and S). The average whitecap coverage for March 1998 in the northern hemisphere is 3.2%, and in the southern hemisphere it is 2.7%.

[54] Retrieving W at several different values of the void fraction α investigates the effect of the void fraction choice. In Figure 6 the distributions and averaged W at $\alpha = 99\%$, 95% , 85% and 60% are compared with those obtained with $\alpha = 98\%$ (equivalent to $Q = 2\%$). The trend is: with α decreasing, the averaged W increases and the distributions become wider, featuring more high W values. The reason is that the lower α (i.e., the more water, Q , the foam contains), the lower foam emissivity e_f until eventually it approaches the value of e_r . With e_f lower, (2) gives higher W . For any α in the range of 95–99%, the distributions do not change significantly, and the averaged W differ at most by 23%. As α approaches 85%, the average W is higher than the previous photographic estimates. At $\alpha = 60\%$, W achieves unrealistically high values, including >1 . In conclusion, void fraction serves as a tuning parameter for the performance of the method and the choice of $\alpha = 98\%$, which is roughly in the middle of the range giving the most reasonable W values, seems appropriate.

[55] For each daily map of W a map of standard deviation, σ_W , is also computed using (10); a relative error for each estimated W value is thus available as σ_W/W in %. The relative errors of estimating W for 27 March 1998 vary widely, from 9% to more than 6,000%. As anticipated from the analytical investigation of the error [*Anguelova*, 2002] and previous experiences [*Blanc*, 1987; *Andreas*, 1991], high error under certain conditions is not a surprise. Rather the question is: what is the acceptable error for W estimation? An arbitrary choice of 30% relative error as a criterion for a reliable estimation of W deems only 48% of all retrieved W values as acceptable, and discards the remaining W values as “bad” data. Moreover, with no exception, all discarded W estimates are for low whitecapping, which certainly creates a bias toward higher values in the distribution of W . To keep the error as low as possible, yet not discard a statistically significant amount of data featuring low W , we decided to use all estimates with standard deviation $\sigma_W \leq W$. Applying this criterion to the W s retrieved for 27 March 1998 leads to the following statistics: (1) only about 5% of all retrieved data is “bad” data with relative error above 100%; (2) about 47% of the retrieved W s have an error from 30% to 100%; and (3) about 48% of the W s have error below 30%. Two points are noteworthy: (1) Indeed, the 5% “bad” data all comprise low W values, but this does not introduce a statistically significant change in the W distributions; (2) The method provides many more W data (about half of the estimates) with an error smaller than 30% compared to the photographically measured W (only about 1/3 of the measurements). Figure 7 shows the distribution of the relative errors of W values retrieved for 27 March 1998. Error statistics of the satellite-measured W for all days in 1998 are similar. The minimum number of cells discarded due to large relative error (above 100%) is

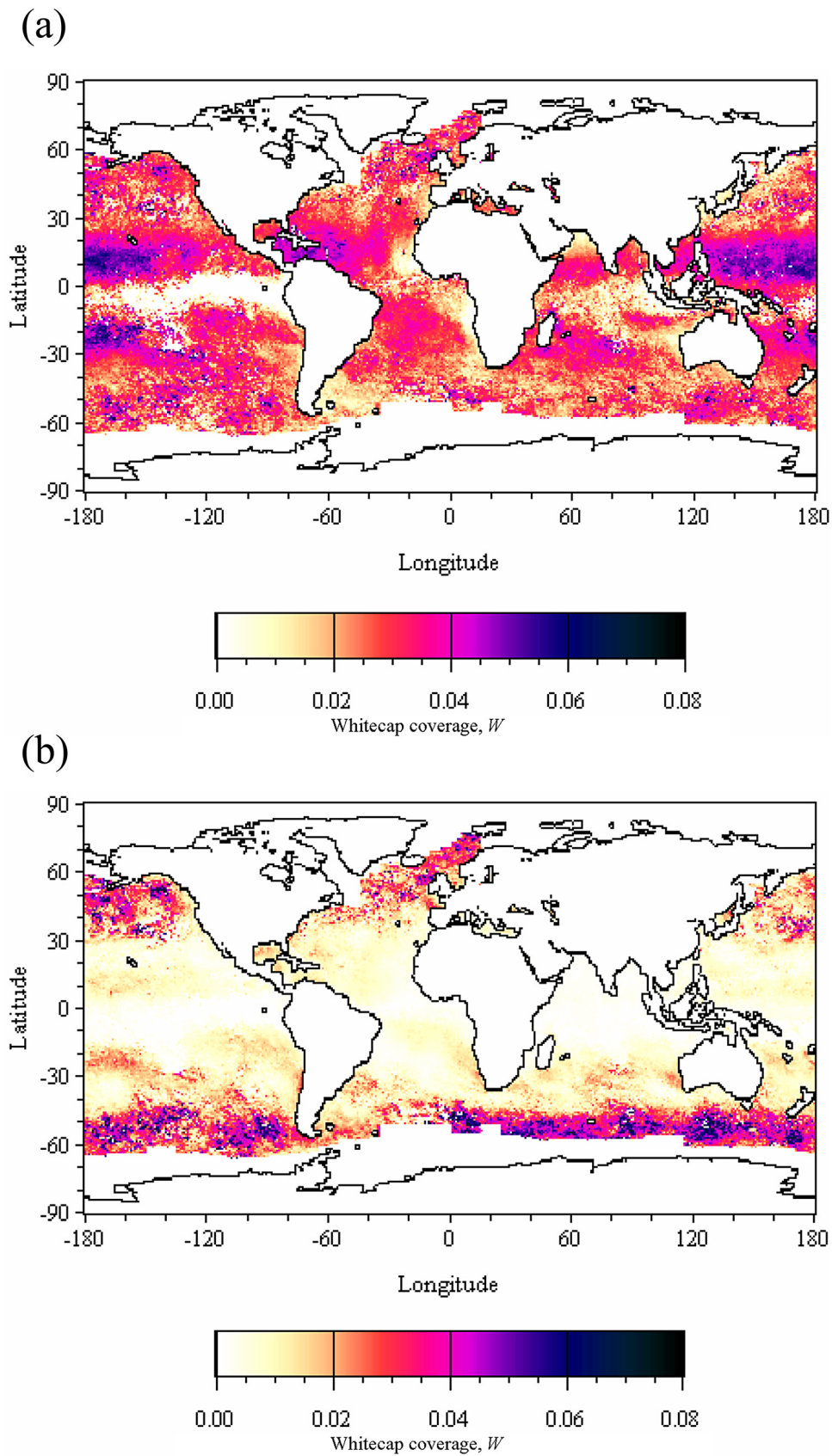


Figure 5. Mean whitecap coverage for March 1998 (average of 31 daily maps of W). Values for W are in fraction, not percent: (a) Obtained from satellite measurements. (b) Computed with wind speed formula (11) and daily fields of wind speed.

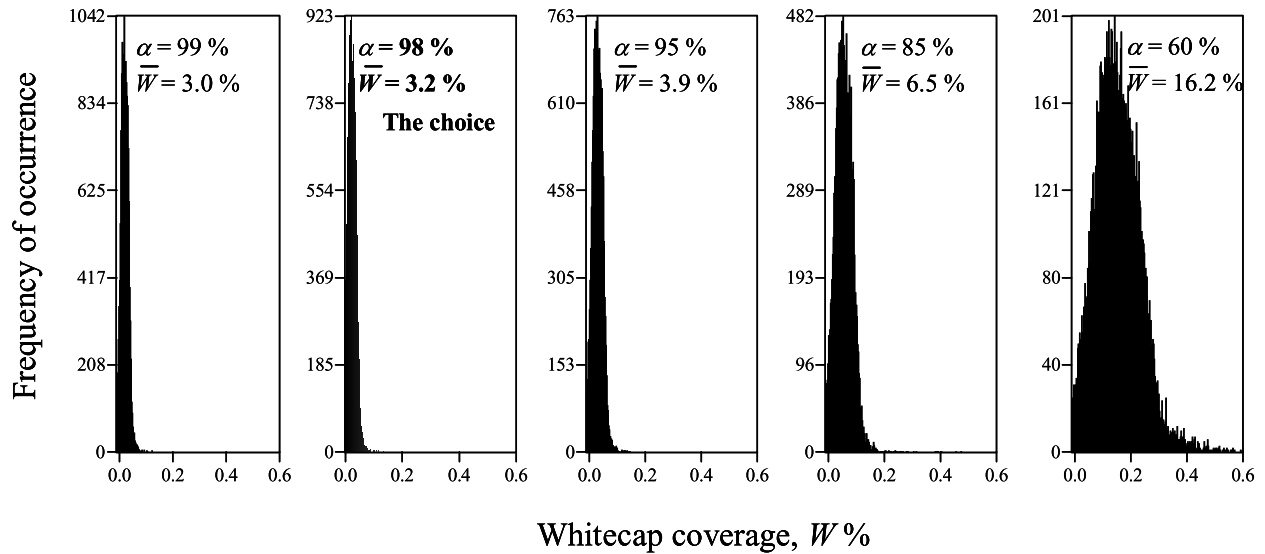


Figure 6. Comparison of the W value distributions at different void fractions α .

encountered in July, about 2.5% of all useful cells. The maximum number of cases with large errors is registered in May, about 10.5% of all useful cells.

[56] While Figure 5a represent the first global whitecap coverage obtained from satellite measurements, the global distribution and seasonal changes of oceanic whitecaps have been previously investigated using $W(U_{10})$ relations [Blanchard, 1963; Spillane et al., 1986; Erickson et al., 1986]. In estimating global whitecap coverage, all authors discuss possible underestimation of W values for two reasons. First, ships usually avoid areas with stormy weather leading to under sampling of high-wind speed conditions

[Spillane et al., 1986]. Second, due to the nonlinearity of the $W(U_{10})$ dependence, the use of mean winds, usually monthly means, instead of instantaneous winds, also yields underestimation of the whitecap coverage. Blanchard [1963, 1983, 1985] and Erickson et al. [1986] account for this problem by correcting their W estimates for the standard deviation of the wind speed.

[57] In this study, whitecap coverage is calculated from daily (in a sense instantaneous) fields of satellite data. The daily values of the whitecap coverage are averaged to obtain monthly, seasonal, or annual means of W . These are used to investigate the spatial and temporal characteristics of the

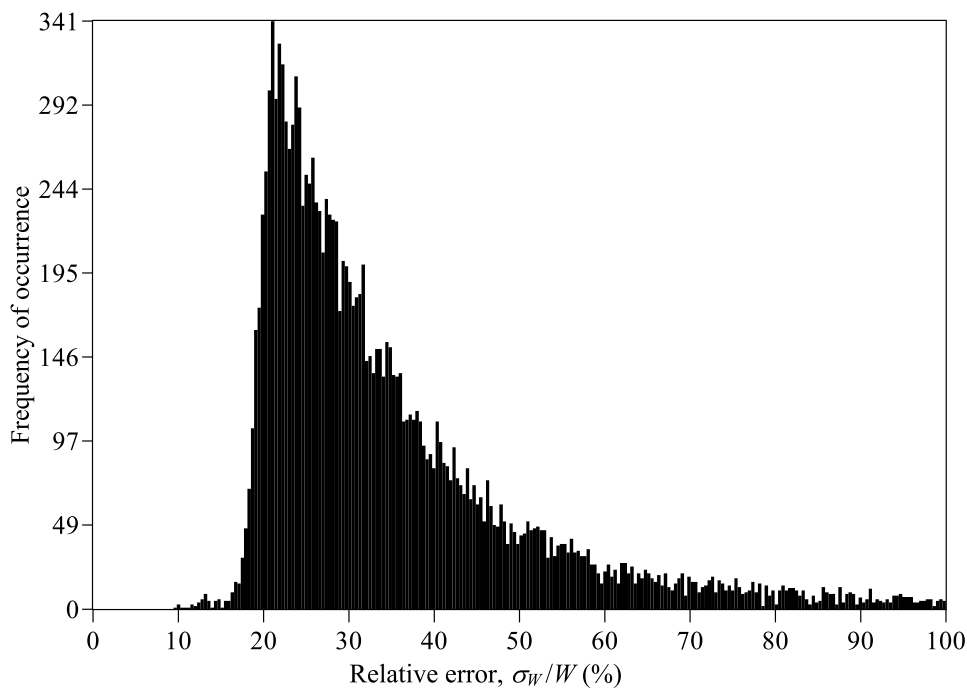


Figure 7. Distribution of the relative errors of retrieving whitecap coverage from satellite data for 27 March 1998.

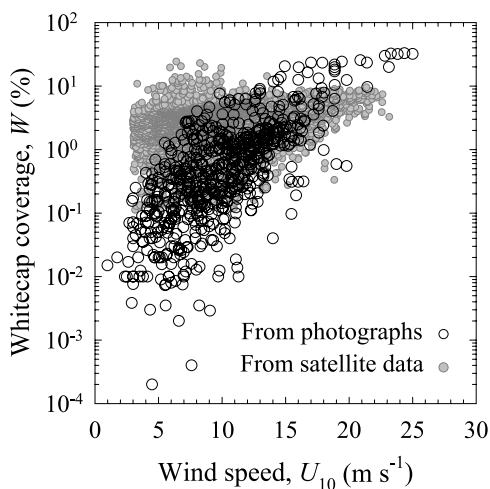


Figure 8. Comparison of photographic measurements of whitecap coverage, W (most of the data sets in Table 2), with satellite-measured W for one day (27 March 1998).

global whitecap coverage [Anguelova, 2002, chap. 4]. Globally averaged annual W obtained with satellite-measured data is estimated to be 3.05%, which is consistent with Blanchard's [1963, Table 3] estimates of 3.4%. Comparisons on more regional scales, however, showed that satellite-retrieved estimates are usually higher than the photographic measurements. One possible reason for these higher values is that the satellite retrievals need an improved computational algorithm. However, it is also possible that the method described gives higher estimates of W because it measures both stages (A and B, i.e., active and decaying) of the whitecaps and uses daily instead of monthly data.

4.2. Evaluation

[58] At this time, the photographic data sets (Table 2) are the only available data for comparison with and evaluation of the satellite-derived whitecap coverage. This comparison cannot be considered a rigorous validation because the spatial resolution of the satellite retrievals is much coarser than that of the photographic measurements. However, such a comparison can be used to illustrate the consistency of the satellite retrievals. Measurements of whitecap coverage from the existing data sets, as a function of wind speed, shown in Figure 3a are replotted in Figure 8 (open circles, 646 points; not all data sets listed in Table 2 are included in the figure) together with W values obtained from satellite measurements for 27 March 1998 (shaded circles, about 14,700 points after removing invalid and erroneous estimates). Generally, the two databases are consistent with regard to absolute values and scatter. Differences between the two data sets are seen, however, and are expected.

[59] Another way to evaluate the performance of the method is to compare satellite-retrieved whitecap coverage with that calculated from existing parameterizations in terms of wind speed. Figure 5b shows results for whitecap coverage obtained with widely recognized and used parameterization of Monahan and O'Muircheartaigh [1980]:

$$W = 3.84 \times 10^{-6} U_{10}^{3.41}. \quad (11)$$

For this calculation we use a global $0.5^\circ \times 0.5^\circ$ map of wind speed for March 1998 (average of 31 daily wind speed maps), which ensures temporal and spatial matching with the satellite-retrieved whitecap coverage shown in Figure 5a. Again, a comparison of Figures 5a and 5b shows a general consistency in absolute values, but with large differences in spatial distribution. It is argued here that while issues with the described implementation probably contribute to these differences (section 5.1), a possible reason is that the satellite-measured whitecap coverage incorporates the effects of environmental variables in addition to wind speed (section 5.2).

5. Discussion

5.1. Implementation Issues

5.1.1. Conditions for Valid and Accurate Estimates

[60] For the day under consideration (27 March 1998), nonphysical negative values for whitecap coverage were computed for 335 cells, about 2.1% of all estimated W values for this day. For the entire 1998, the minimum occurrences of nonphysical negative values for W happened in November with about 0.5% of all useful cells. The maximum number of nonphysical negative values occurred in July, when W values were negative for 7% of all useful cells. Since values for foam emissivity e_f in (2) are consistently high, we compared values of composite surface emissivity e and foam-free emissivity $e_r = e_s + \Delta e_r$ in order to identify the cause for these cases. Figure 9a plots data for e (open circles) and $e_s + \Delta e_r$ (squares) as a function of corresponding brightness temperatures for 27 March 1998 along a north-south line at 83°E . In most cases $e \geq e_s + \Delta e_r$, as it should be, but there are several cases at the highest T_B (from 165 to 168°K) for which $e < e_s + \Delta e_r$ (solid circles). Figures 9b and 9c show that these same low e values are associated with low winds, up to 5.2 m s^{-1} , and high V_s , 63 to 66 mm.

[61] Pandey and Kakar [1982] also encountered negative values for W in their microwave emissivity model. There are two possible causes in their model that can lead to $W < 0$: (1) they use the Stogryn [1972] expression for foam emissivity, which underestimates e_f ; (2) they use T_B data from the SMMR, which is known to have calibration problems [Wentz and Francis, 1992], thus affecting their values for e . According to our investigation, however, even if T_B is well calibrated and a more comprehensive model is used for e_f , cases of $W < 0$ still would occur. Pandey and Kakar [1982] fixed the problem by subtracting a frequency-dependent bias from Hollinger's expressions (7) for roughness emissivity and adding a bias to the Stogryn's [1972] expression for foam emissivity. Knowing that we have not chosen the most comprehensive models for this study, we decided to investigate but not correct the problem with negative W ; at this time we discard all pixels for which $W < 0$.

[62] Figure 9 helps identify one possible combination of conditions that might lead to unreliable detection of e and W : low wind speed coupled with high humidity, situations usually found at low latitudes. Examination of more cases of $e < e_s + \Delta e_r$, however, reveals that these conditions are not the only ones restricting the retrieval of valid and accurate e and W . Too low e values are encountered also

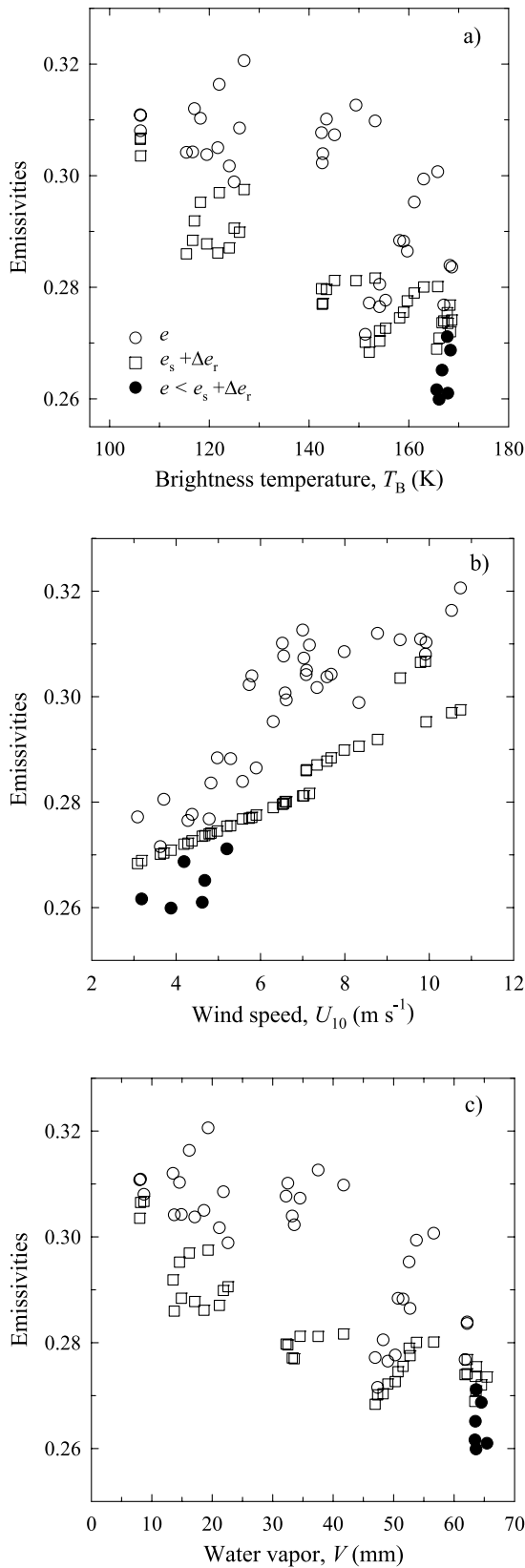


Figure 9. Estimated composite and rough sea emissivities, e and $e_s + \Delta e_r$, observed on 27 March 1998 along the north-south line at 83°E over the range of corresponding (a) brightness temperature, T_B , (b) wind speed, U_{10} , and (c) water vapor, V .

in cases characterized with moderate winds ($7\text{--}10 \text{ m s}^{-1}$) and not so high humidity ($20\text{--}35 \text{ mm}$) at mid latitudes (Figures 10a–10c). It proved difficult to identify a few specific combinations of variables (wind, humidity, water temperature, salinity) responsible for invalid or inaccurate e and W . Instead, numerous restricting conditions are encountered all over the globe. This suggests that drawbacks of the method, not physical reasons, limit the validity and accuracy of whitecap coverage estimates.

5.1.2. Modeling and Validation

[63] We used simplified models for the emissivities of rough sea and foam, e_r and e_f . While these simple models provide clear separation between e_r and e_f , they may not determine the rough and foam emissivities accurately. The masking of the surface emissivity signal in low-wind/high-humidity conditions revealed in Figure 9 points to the importance of the atmospheric correction model used to compute e . In addition, after applying the clear sky mask, we assumed $L \cong 0$ and $a_L \cong 0$, which may not always hold true. While we did that to avoid the high uncertainty in retrieving L , completely neglecting the effect of the remaining cloud liquid water may introduce some error. Also, by necessity because of the lack of other data at the time of this study, the satellite brightness temperatures and the correction parameters needed to derive e , namely water vapor, V , and cloud liquid water, L , were obtained from the same satellite data set (SSM/I). Therefore the satellite-retrieved whitecap coverage could be somewhat dependent on the assumptions made in the SSM/I retrieval algorithm.

[64] The most rigorous way to evaluate the performance of the method estimating whitecap coverage from satellite measurements is to investigate the bias, ΔW , between satellite-measured whitecap coverage, W_{sat} , and true whitecap coverage, W_{true} : $\Delta W = W_{sat} - W_{true}$. If W_{true} is reliably and accurately measured, then the bias ΔW will be mainly due to issues with the models and data used to obtain the emissivities in (2). Thus the accuracy of W_{sat} can be evaluated and eventually increased with improvements in models and data sets used (see section 5.3). At this time, however, the magnitude of the bias ΔW cannot serve as a fair measure for the performance of the method because, besides the modeling and data issues listed in the previous paragraph that influence W_{sat} , ΔW is also affected by uncertainties in W_{true} . True whitecap coverage can be represented either by photographic and video measurements or by predictions from a reliable $W(U_{10})$ relation. We have shown, however, that existing photographic measurements of whitecap coverage do not fully represent different conditions over the globe (section 2.4) and relation $W(U_{10})$ cannot model the whitecap coverage variability adequately (section 2.3). Though slowly, new photographic measurements of whitecap coverage will improve W_{true} and provide data for direct validation of W_{sat} . Meanwhile, the main approach to minimize ΔW is to improve modeling and data usage to obtain W_{sat} .

5.2. New Physical Insights

[65] Fully aware of the issues discussed in section 5.1, yet encouraged by the overall consistency between satellite estimates and photographic measurements in Figure 8, we believe that the satellite-based estimates of W can provide new physical insights into global whitecap coverage, which

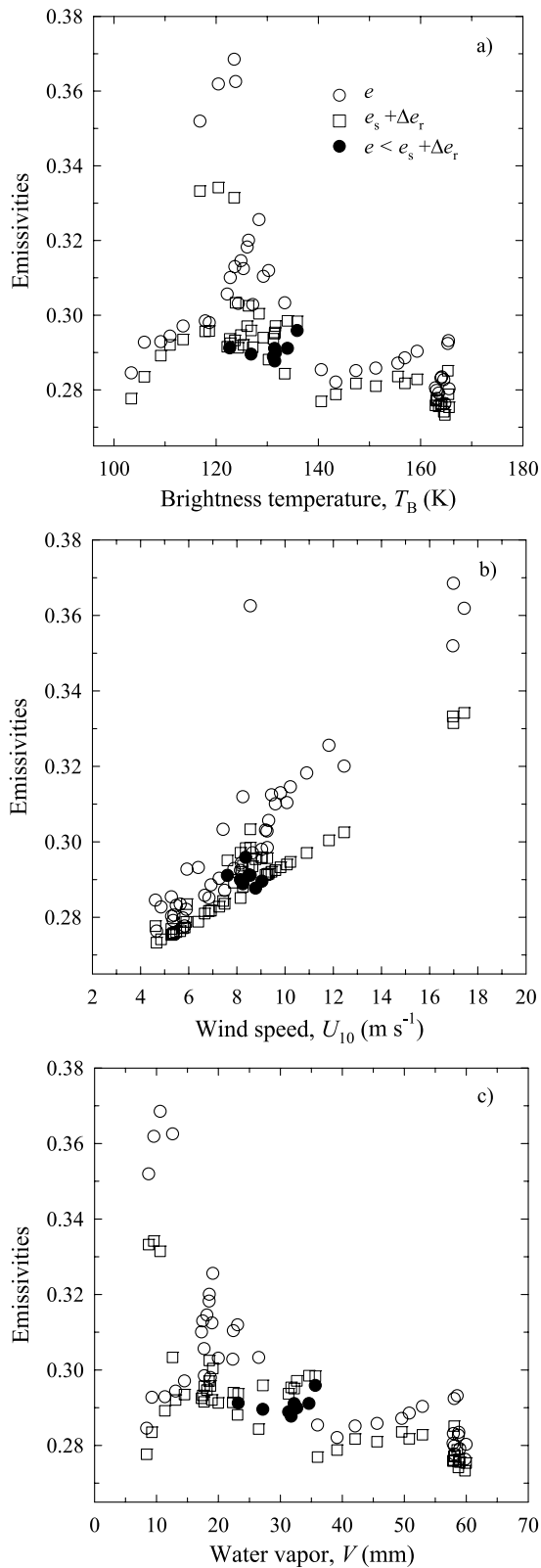


Figure 10. Estimated composite and rough sea emissivities, e and $e_s + \Delta e_r$, observed on 27 March 1998 along the north-south line at 8°E over the range of corresponding: (a) brightness temperature, T_B , (b) wind speed, U_{10} , and (c) water vapor, V .

the available photographic data and the $W(U_{10})$ parameterization do not capture well. Figures 5 and 8 support our interpretation.

[66] First, the wind speed dependence of the satellite and photographically derived W values in Figure 8 are somewhat different, with the photographically derived W increasing more rapidly with wind speed than the satellite-retrieved measurements. Our error analysis shows that higher error is associated with low estimates of whitecap coverage at low winds, while at high winds the error is consistently lower. Thus, in explaining the difference in wind speed dependence between satellite and photographically derived W values, we look into physical rather than implementation reasons. The slower changes of satellite-derived W with U_{10} can be interpreted as a result of suppression of the action of strong winds and boosting of the action of moderate winds by local meteorological and environmental conditions. Second, satellite-retrieved whitecap coverage clearly shows the expected high variability of W at moderate winds (6 to 12 m s^{-1}).

[67] The differences apparent in Figure 8 are manifested as different global distributions in Figures 5a and 5b. As (11) suggests, the conventional $W(U_{10})$ relation inevitably predicts high whitecap coverage in high latitudes, around 50° – 60°N and S (Figure 5b) because average wind speed is high in these regions. In mid and low latitudes, where the wind speeds are lower, the whitecapping is rarely above 1%. Same features (high W at high latitudes, low W at low latitudes) are observed in *Spillane et al.*'s [1986, Figure 5] climatological whitecap atlas for March since it was produced with an approach similar to (11). These observations are in contrast to the picture in Figure 5a where no such strong gradient from high to low latitudes is observed. Instead, high variability in values makes whitecap coverage more uniform latitudinally: not very high at high latitudes and higher at mid and even low latitudes.

[68] Though strikingly different from the global distribution predicted by (11) and documented by *Spillane et al.*'s [1986] climatological whitecap atlas, the features of satellite-derived whitecap coverage in Figure 5a can be explained with the effects of various environmental factors whose concerted action enhances the effect of wind alone in some regions and suppresses wind action in others. For example, it is expected that, with all other conditions similar, whitecap coverage would be higher at 12 m s^{-1} wind in warm waters than whitecap coverage at 12 m s^{-1} wind in cold waters due to water viscosity differences. Indeed, Figure 5a shows that satellite-derived whitecap coverage in the Southern Ocean and the northern reaches of the North Atlantic and North Pacific is not the highest because these are regions where high winds are invariably coupled with very low water temperatures (often below 0°C). Furthermore, the persistent trade winds and the long fetches in the tropics further foster whitecapping in warm waters. Also, the central parts of the oceans, regions of downwelling of warm surface waters, are oligotrophic [Pinet, 1992, p. 376] as nutrients are exported from the surface layer. A low concentration of organisms in places with less nutrients leads, presumably, to a low concentration of surface-active materials, thus wave breaking in these warm waters is not suppressed by surfactants and whitecapping is enhanced. In contrast, coastal upwelling west of

Africa and South America, as well as Polar upwelling in the Southern Ocean [Pinet, 1992, p. 388, Figure 12–1], brings cold nutrient-laden waters at the surface leading to high primary production, thus more surfactants in the surface water, which would hinder wave breaking and diminish whitecapping.

[69] It is anticipated that addressing rigorously the modeling and data issues discussed in section 5.1.2 may reduce the strength of or even change the spatial features in Figure 5a to some extent. We suspect, though, that fingerprints of various factors affecting whitecap coverage will still be discernable and the global spatial distribution of satellite-measured whitecap coverage will still be different from that obtained with $W(U_{10})$ relation. This, however, remains to be seen.

[70] An independent and completely different study corroborates the global distribution of satellite-measured whitecap coverage revealed in Figure 5a. Haywood et al. [1999] computed the solar irradiance at the top of the atmosphere in several runs of general circulation model (GCM). Once they ran their GCM without any atmospheric aerosols, then in several additional GCM runs they introduced different combinations of aerosols both natural and anthropogenic. For each GCM run, the model results for solar irradiance were compared with those observed by the Earth Radiation Budget Experiment (ERBE). Without aerosols, their GCM underestimated the solar irradiance over the entire globe (Haywood et al.'s Figure 1A). When all aerosol types except sea-salt aerosols were introduced, the bias between GCM predictions and ERBE measurements was only partially eliminated (Haywood et al.'s Figure 1B). The inclusion of sea-salt aerosols with low concentration further decreased but did not fully eradicate the bias between model and measurements (Haywood et al.'s Figure 1C). Sea-salt aerosols with high concentration brought the best balance between model and measurements at low and mid latitudes, but at high latitudes the model overestimated the solar irradiance (Haywood et al.'s Figure 1D). The point of this description is that in Haywood et al.'s figures the solar irradiance exhibits a global spatial distribution whose main features closely resemble those of whitecap coverage in our Figure 5a. This implies that sea-salt aerosols, and perhaps whitecaps albedo as well, are most necessary for the reflected radiance in the same places where we observe high whitecap coverage, which would be the main initial source for sea-salt aerosols.

5.3. Possible Improvements

[71] The discussion in section 5.1.2 points to two major necessary improvements, namely more comprehensive models for the emissivities in (2) and decoupled data sets for the computations. To minimize correlations and error propagation, it is preferable to use independent data sets for the brightness temperature and atmospheric correction variables to obtain the composite emissivity e (equations (4)–(5)). The recent launch of WindSat [Gaiser et al., 2004] should make this possible. For instance, we can use brightness temperatures from the WindSat sensor and make the atmospheric correction employing data for water vapor and cloud liquid water from SSM/I. Similarly, it is desirable to decouple the quantities used in the models for e_r and e_f (e.g., SST taken from weather forecast analyses) from those

directly measured and used to obtain e (e.g., SST from AVHRR). Using various independent data sets, however, raises the necessity of their rigorous matchup in time and space with a potential to introduce a significant source of error.

[72] Calculations of the emissivity of rough sea surface, $e_r = e_s + \Delta e_r$, should be placed on a more sound physical ground. Instead of the empirical expression used in this implementation for surface roughness correction Δe_r , the so-called two-scale emissivity model can be used to compute e_r [Wentz, 1983; Durden and Vesecky, 1985; Yueh, 1997, St. Germain et al., 2002]. This model best describes changes of ocean emissivity for winds up to 10–12 m s⁻¹ due to Bragg scattering from short gravity and capillary waves riding on long waves with a Gaussian distribution of slopes. Gains from a better physical model, however, will raise new issues. Though the two-scale model has matured over the years since its first introduction [Semyonov, 1966], it has limitations such as the choices of the wavelength separating short and long waves and of the wave spectrum model [Zhang and Johnson, 2001]. Another anticipated challenge is the clear separation of e_r and e_f in (1). Therefore new theories and models [Johnson, 2002] should also be considered.

[73] The emissivity of foam, e_f , which is modeled with the Fresnel formula for foam reflectivity, also needs improvement. The assumption in this model of constant void fraction, α , throughout the foam layer at the surface and the chosen value of $\alpha = 98\%$ ensure a fair prediction of the emissivity of thick, freshly generated whitecaps (stage A), but it is only partially suitable for aged thinner whitecaps in stage B. Since the area of the aged whitecaps is much larger than the area of fresh thick ones, a realistic physical model should have a way to account for the characteristics and emission of both types of whitecaps. A model for e_f incorporating void fraction changes with depth and distribution of foam thicknesses can address this requirement.

6. Conclusions

[74] The necessity to model realistically the high variability of whitecap coverage has justified the development of a method for estimating whitecap coverage on a global scale from routinely measured satellite data as an alternative to traditional photographic measurements. The concept for satellite-based estimates of W relies on changes of microwave brightness temperature at 19 GHz (horizontal polarization) at the ocean surface as whitecap coverage increases. Models, parameterizations, data sets, and assumptions used to implement the method are described. Though highly simplified, this initial implementation proves the feasibility of the concept. It should be possible to obtain daily global whitecap coverage estimates with an error of at most one standard deviation. Drawbacks of the method are analyzed and necessary changes and improvements are discussed.

[75] Satellite-derived values for whitecap coverage are of the same order of magnitude as those from previous photographic measurements, but their global distribution is quite different from that predicted from conventional relations using wind speed. This different spatial distribution is plausibly explainable through the effects of various

Table A1. Variances of the Basic Variables Contributing to the Errors of Emissivities (A2)

Standard Deviation for Variable	Symbol	Value	Units	Reference
Brightness temperature	σ_{T_B}	1	K	Wentz [1997]
Sea surface temperature	σ_{T_s}	0.3	K	data
Water salinity	σ_S	0.2	psu	data
Water vapor	σ_V	1.2	mm	Wentz [1997]
Wind speed	σ_U	0.9	m s^{-1}	Wentz [1997]
Incident angle	σ_θ	0.25	deg	Wentz [1997]
Dielectric constant at infinite frequency	$\sigma_{\varepsilon_\infty}$	0.98		Stewart [1985]
Conductivity	σ_σ	4.41	$\Omega^{-1} \text{m}^{-1}$	chosen
Water fraction	σ_Q	1	%	chosen

meteorological and environmental factors in addition to the effect of wind alone. Using satellite-based estimates, an extensive database of whitecap coverage under a myriad of conditions encountered over the globe can be assembled. Such a database might be used to improve existing, or to develop new, models and parameterizations for various air-sea interaction processes such as the production of sea-salt aerosols and gas transfer.

Appendix A: Error Analysis—Sensitivity Coefficients and Variances

[76] The sensitivity coefficients in (10) are

$$\begin{aligned}
 W_e &= \frac{1}{(e_f - e_s - \Delta e_r)^2}, & W_f &= \frac{(e - e_s - \Delta e_r)^2}{(e_f - e_s - \Delta e_r)^4}, \\
 W_s &= \frac{(e - e_f)^2}{(e_f - e_s - \Delta e_r)^4}, & W_{er} &= \frac{e - e_f}{(e_f - e_s - \Delta e_r)^3}, \\
 W_r &= \frac{(e - e_f)^2}{(e_f - e_s - \Delta e_r)^4} \equiv W_s, & W_{sf} &= -\frac{(e - e_f)(e - e_s - \Delta e_r)}{(e_f - e_s - \Delta e_r)^4}.
 \end{aligned} \tag{A1}$$

[77] The variances of the four emissivities in (10) are

$$\begin{aligned}
 \sigma_e^2 &\leq E_{eB}\sigma_{T_B}^2 + E_{eT}\sigma_{T_s}^2 + E_{eV}\sigma_V^2 + E_{e\theta}\sigma_\theta^2 \\
 &\quad + 2E_{BV}\sigma_{T_B}\sigma_V + 2E_{B\theta}\sigma_{T_B}\sigma_\theta + 2E_{V\theta}\sigma_V\sigma_\theta \\
 \sigma_{e_s}^2 &= E_{sT}\sigma_{T_s}^2 + E_{sS}\sigma_S^2 + E_{s\theta}\sigma_\theta^2 + E_{s\sigma}\sigma_\sigma^2 + E_{s\infty}\sigma_{\varepsilon_\infty}^2 \\
 \sigma_{e_f}^2 &= E_{fT}\sigma_{T_s}^2 + E_{fS}\sigma_S^2 + E_{f\theta}\sigma_\theta^2 + E_{f\sigma}\sigma_\sigma^2 + E_{f\infty}\sigma_{\varepsilon_\infty}^2 + E_{fQ}\sigma_Q^2 \\
 \sigma_{e_r}^2 &\leq E_{rT}\sigma_{T_s}^2 + E_{rU}\sigma_U^2 + E_{r\theta}\sigma_\theta^2 + 2E_{U\theta}\sigma_U\sigma_\theta
 \end{aligned} \tag{A2}$$

In (A2), E_{ej} , E_{sj} , E_{fj} , and E_{rj} are the sensitivity coefficients for e , e_s , e_f , and Δe_r , respectively. The index j show the basic variables contributing to the emissivity errors. Each of the sensitivity coefficients, E_{ij} , is determined by a set of expressions containing numerous terms (not shown). The inequality signs in (10) and (A2) come from Schwarz inequality, $|\sigma_{uv}^2| \leq \sigma_u\sigma_v$.

[78] Table A1 lists the standard deviations (or RMS errors), σ_x , of the variables used to compute emissivity variances in (A1)–(A2).

[79] **Acknowledgments.** This work was done while the first author was completing her Ph.D. at the College of Marine Studies, University of Delaware, and was partly supported by the NSF Ocean Sciences Division under grant OCE-9730439. The authors wish to thank the reviewers whose careful review of the manuscript and detailed suggestions and comments

helped improve the text. M.A. wishes to thank Michael Bettenhausen (NRL, Remote Sensing Division) for valuable discussions on the remote sensing part of the paper.

References

- Alpers, W., and H. Hühnerfuss (1989), The damping of ocean waves by surface films: A new look at an old problem, *J. Geophys. Res.*, *94*, 6251–6265.
- Andreae, M. (1995), Climatic effects of changing atmospheric aerosol levels, in *World Survey of Climatology*, vol. 16, *Future Climates of the World*, edited by A. Henderson-Sellers, pp. 347–398, Elsevier, New York.
- Andreas, E. (1991), Using scintillation at two wavelengths to measure path-averaged heat fluxes in free convection, *Boundary Layer Meteorol.*, *54*, 167–182.
- Andreas, E. (1992), Sea spray and the turbulent air–sea heat fluxes, *J. Geophys. Res.*, *97*, 11,429–11,441.
- Andreas, E. (2002), A review of the sea spray generation function for the open ocean, in *Atmosphere–Ocean Interactions, Adv. Fluid Mech.*, vol. 33, edited by W. Perrie, pp. 1–46, WIT, Boston, Mass.
- Andreas, E., and K. Emanuel (2001), Effects of sea spray on tropical cyclone intensity, *J. Atmos. Sci.*, *58*, 3741–3751.
- Andreas, E., J. Edson, E. Monahan, M. Rouault, and S. Smith (1995), The spray contribution to the net evaporation from the sea: A review of recent progress, *Boundary Layer Meteorol.*, *72*, 3–52.
- Anguelova, M. (1997), Laboratory study of bubble clouds characteristics at various conditions, M. S. thesis, 255 pp., Univ. of Del., Lewes.
- Anguelova, M. (2002), Whitecaps, sea-salt aerosols, and climate, Ph.D. thesis, 248 pp., Univ. of Del., Lewes.
- Asher, W., and R. Wanninkhof (1998), The effects of bubble-mediated gas transfer on purposeful dual-gaseous tracer experiment, *J. Geophys. Res.*, *103*, 10,555–10,560.
- Asher, W., J. Edson, W. McGillis, R. Wanninkhof, D. Ho, and T. Litchendorf (2002), Fractional area whitecap coverage and air–sea gas transfer velocities measured during GasEx-98, in *Gas Transfer at Water Surfaces, Geophys. Monogr. Ser.*, vol. 127, edited by M. Donelan et al., pp. 199–204, AGU, Washington, D. C.
- Barrie, L., J. Bottenheim, R. Schnell, P. Crutzen, and R. Rasmussen (1988), Ozone destruction and photochemical reactions at polar sunrise in the lower Arctic atmosphere, *Nature*, *334*, 138–141.
- Bevington, P. (1969), *Data Reduction and Error Analysis for the Physical Sciences*, 336 pp., McGraw-Hill, New York.
- Blanc, T. (1987), Accuracy of bulk-method-determined flux, stability, and sea surface roughness, *J. Geophys. Res.*, *92*, 3867–3876.
- Blanchard, D. (1963), The electrification of the atmosphere by particles from bubbles in the sea, *Prog. Oceanogr.*, *1*, 71–202.
- Blanchard, D. (1983), The production, distribution and bacterial enrichment of the sea-salt aerosol, in *Air–Sea Exchange of Gases and Particles*, edited by P. Liss and G. Slinn, pp. 407–454, Springer, New York.
- Blanchard, D. (1985), The oceanic production of atmospheric sea salt, *J. Geophys. Res.*, *90*, 961–963.
- Bondur, V., and E. Sharkov (1982), Statistical properties of whitecaps on a rough sea, *Oceanology*, *22*, 274–279.
- Bortkovskii, R. (1987), *Air–Sea Exchange of Heat and Moisture During Storms*, 193 pp., Springer, New York.
- Bourassa, M. (2004), An improved sea state dependency for surface stress derived from in situ and remotely sensed winds, *Adv. Space Res.*, *33*, 1136–1142.
- Camps, A., et al. (2002), Sea surface emissivity observations at L-band: First results of the Wind and Salinity Experiment WISE 2000, *IEEE Trans. Geosci. Remote Sens.*, *40*, 2117–2130.
- Camps, A., et al. (2004), The WISE 2000 and 2001 field experiments in support of the SMOS mission: Sea surface L-band brightness temperature observations and their application to sea surface salinity retrieval, *IEEE Trans. Geosci. Remote Sens.*, *42*, 804–823.

- Cardone, V. J. (1969), Specification of the wind distribution in the marine boundary layer for wave forecasting, *Tech. Rep. 69-1*, 131 pp., Geophys. Sci. Lab., N. Y. Univ., New York.
- Cartmill, J., and M. Su (1993), Bubble size distribution under saltwater and freshwater breaking waves, *Dyn. Atmos. Oceans*, 20, 25–31.
- Chameides, W., and A. Stelson (1992), Aqueous-phase chemical processes in deliquescent sea-salt aerosols: A mechanism that couples the atmospheric cycles of S and sea salt, *J. Geophys. Res.*, 97(D18), 20,565–20,580.
- Charlson, R., J. Lovelock, M. Andreae, and S. Warren (1987), Oceanic phytoplankton, atmospheric sulfur, cloud albedo and climate, *Nature*, 326, 655–661.
- Chen, D., L. Tsang, L. Zhou, S. Reising, W. Asher, L. Rose, K.-H. Ding, and C.-T. Chen (2003), Microwave emission and scattering of foam based on Monte Carlo simulations of dense media, *IEEE Trans. Geosci. Remote Sens.*, 41, 782–790.
- Clegg, N., and R. Toumi (1998), Non-sea-salt-sulphate formation in sea-salt aerosol, *J. Geophys. Res.*, 103, 31,095–31,102.
- Dahl, P., and A. Jessup (1995), On bubble clouds produced by breaking waves: An event analysis of ocean acoustic measurements, *J. Geophys. Res.*, 100, 5007–5020.
- Donelan, M., F. Dobson, S. Smith, and R. Anderson (1993), On the dependence of sea surface roughness on wave development, *J. Phys. Oceanogr.*, 23, 2143–2149.
- Doyle, D. (1984), Whitecaps and the marine atmosphere, *Rep. 6*, 140 pp., Univ. Coll., Galway, Ireland.
- Droppleman, J. (1970), Apparent microwave emissivity of sea foam, *J. Geophys. Res.*, 75, 696–698.
- Durden, S., and J. Vesceky (1985), A physical radar cross-section model for a wind-driven sea with swell, *IEEE J. Oceanic Eng.*, 10, 445–451.
- Emery, W., S. Castro, G. Wick, P. Schlüssel, and C. Donlon (2001), Estimating sea surface temperature from infrared satellite and in situ temperature data, *Bull. Am. Meteorol. Soc.*, 82(12), 2773–2785.
- Erickson, D., III, J. Merrill, and R. Duce (1986), Seasonal estimates of global oceanic whitecap coverage, *J. Geophys. Res.*, 91, 12,975–12,977.
- Fairall, C., J. Keppert, and G. Holland (1994), The effect of sea spray on surface energy transport over the ocean, *Global Atmos. Ocean Syst.*, 2, 121–142.
- Fairall, C., E. Bradley, D. Rogers, J. Edson, and G. Young (1996), Bulk parameterization of air-sea fluxes for Tropical Ocean–Global Atmosphere Coupled-Ocean Atmosphere Response Experiment, *J. Geophys. Res.*, 101, 3747–3764.
- Fairall, C., J. Hare, J. Edson, and W. McGillis (2000), Parameterization and micrometeorological measurement of air-sea gas transfer, *Boundary Layer Meteorol.*, 96, 63–106.
- Finlayson-Pitts, B., and J. Pitts Jr. (1997), Tropospheric air pollution: Ozone, airborne toxics, polycyclic aromatic hydrocarbons, and particles, *Science*, 276, 1045–1052.
- Frew, N. (1997), The role of organic films in air-sea gas exchange, in *The Sea Surface and Global Change*, edited by P. Liss and R. Duce, pp. 121–172, Cambridge Univ. Press, New York.
- Frouin, R., M. Schwindling, and P.-Y. Deschamps (1996), Spectral reflectance of sea foam in the visible and near-infrared: In situ measurements and remote sensing implications, *J. Geophys. Res.*, 101, 14,361–14,371.
- Frouin, R., S. Iacobellis, and P.-Y. Deschamps (2001), Influence of oceanic whitecaps on the global radiation budget, *Geophys. Res. Lett.*, 28, 1523–1526.
- Gaiser, P., et al. (2004), The WindSat spaceborne polarimetric microwave radiometer: Sensor description and early orbit performance, *IEEE Trans. Geosci. Remote Sens.*, 42, 2347–2361.
- Garrett, W. (1967), Stabilization of air bubbles at the air-sea interface by surface-active material, *Deep Sea Res.*, 14, 661–672.
- Ghan, S., G. Guzman, and H. Abdul-Razzak (1998), Competition between sea salt and sulfate particles as cloud condensation nuclei, *J. Atmos. Sci.*, 55, 3340–3347.
- Goodberlet, M., C. Swift, and J. Wilkerson (1989), Remote sensing of ocean surface winds with the Special Sensor Microwave/Imager, *J. Geophys. Res.*, 94, 14,547–14,555.
- Gordon, H., and M. Jacobs (1977), Albedo of the ocean-atmosphere system: Influence of sea foam, *Appl. Opt.*, 16, 2257–2260.
- Gordon, H., and M. Wang (1994), Influence of oceanic whitecaps on atmospheric correction of ocean-color sensors, *Appl. Opt.*, 33, 7754–7763.
- Grini, A., G. Myhre, J. Sundet, and I. Isaksen (2002), Modeling the annual cycle of sea salt in the global 3D model Oslo CTM2: Concentrations, fluxes, and radiative impact, *J. Clim.*, 15, 1717–1730.
- Hanson, J., and O. Phillips (1999), Wind sea growth and dissipation in the open ocean, *J. Phys. Oceanogr.*, 29, 1633–1648.
- Hasted, J. (1973), *Aqueous Dielectrics*, CRC Press, Boca Raton, Fla.
- Haywood, J., V. Ramaswamy, and B. Soden (1999), Tropospheric aerosol climate forcing in clear-sky satellite observations over the oceans, *Science*, 283, 1299–1303.
- Hollinger, J. (1971), Passive microwave measurements of sea surface roughness, *IEEE Trans. Geosci. Electron.*, 9, 165–169.
- Hollinger, J., J. Peirce, and G. Poe (1990), SSM/I instrument evaluation, *IEEE Trans. Geosci. Remote Sens.*, 28, 781–790.
- Hühnerfuss, H., W. Walter, P. Lange, and W. Alpers (1987), Attenuation of wind waves by monomolecular sea slicks and the Marangoni effect, *J. Geophys. Res.*, 92, 3961–3963.
- Jacobson, M. (2001), Global direct radiative forcing due to multicomponent anthropogenic and natural aerosols, *J. Geophys. Res.*, 106(D2), 1551–1568.
- Johnson, J. (2002), Comparison of the physical optics and small slope theories for polarimetric thermal emission from the sea surface, *IEEE Trans. Geosci. Remote Sens.*, 40, 500–504.
- Kawanishi, T., T. Sezai, Y. Ito, K. Imaoka, T. Takeshima, Y. Ishido, A. Shibata, M. Miura, H. Inahata, and R. W. Spencer (2003), The advanced microwave scanning radiometer for the Earth observing system (AMSR-E), NASA's contribution to the EOS for global energy and water cycle studies, *IEEE Trans. Geosci. Remote Sens.*, 41, 184–194.
- Keene, W., A. A. Pszenny, D. Jacob, R. Duce, J. Galloway, J. Schultz-Tokos, H. Sievering, and J. Boatman (1990), The geochemical cycling of reactive chlorine through the marine troposphere, *Global Biogeochem. Cycles*, 4, 407–430.
- Klein, L., and C. Swift (1977), An improved model for the dielectric constant of sea water at microwave frequencies, *IEEE Trans. Antennas Propag.*, 25, 104–111.
- Koepke, P. (1984), Effective reflectance of oceanic whitecaps, *Appl. Opt.*, 23, 1816–1824.
- Koepke, P. (1986), Remote sensing signature of whitecaps, in *Oceanic Whitecaps and Their Role in Air–Sea Exchange Processes*, edited by E. Monahan and G. M. Niocaill, pp. 251–260, Springer, New York.
- Kokhanovsky, A. (2004), Spectral reflectance of whitecaps, *J. Geophys. Res.*, 109, C05021, doi:10.1029/2003JC002177.
- Kondo, J., Y. Fujinawa, and G. Naito (1973), High-frequency components of ocean waves and their relation to the aerodynamic roughness, *J. Phys. Oceanogr.*, 3, 197–202.
- Koop, T., A. Kapilashrami, L. Molina, and M. Molina (2000), Phase transitions of sea-salt/water mixtures at low temperatures: Implications for ozone chemistry in the polar marine boundary layer, *J. Geophys. Res.*, 105(D21), 26,393–26,402.
- Kraan, C., W. Oost, and P. Janssen (1996), Wave energy dissipation by whitecaps, *J. Atmos. Oceanic Technol.*, 13, 262–267.
- Lafon, C., J. Piazzola, P. Forget, O. le Calve, and S. Despiau (2004), Analysis of the variations of the whitecap fraction as measured in a coastal zone, *Boundary Layer Meteorol.*, 111, 339–360.
- Large, W., and S. Pond (1981), Open ocean momentum flux measurements in moderate to strong winds, *J. Phys. Oceanogr.*, 11, 324–336.
- Levitus, S., T. Boyer, M. Conkright, T. O'Brien, J. Antonov, C. Stephens, L. Stathopoulos, D. Johnson, and R. Gelfeld (1998), *World Ocean Database 1998*, vol. 1, *Introduction*, NOAA Atlas NESDIS 18, 346 pp., NOAA, Silver Spring, Md.
- Liao, H., J. Seinfeld, P. Adams, and L. Mickley (2004), Global radiative forcing of coupled tropospheric ozone and aerosols in a unified general circulation model, *J. Geophys. Res.*, 109, D24204, doi:10.1029/2004JD005476.
- Liss, P., and L. Merlivat (1986), Air-sea gas exchange rates: Introduction and synthesis, in *The Role of Air–Sea Exchange in Geochemical Cycling*, edited by P. Baut-Menard, pp. 113–127, Springer, New York.
- Liu, W., K. Katzaros, and J. Businger (1979), Bulk parameterization of air-sea exchange of heat and water vapor including the molecular constraints at the interface, *J. Atmos. Sci.*, 36, 1722–1735.
- Luria, M., and H. Sievering (1991), Heterogeneous and homogeneous oxidation of SO₂ in the remote marine atmosphere, *Atmos. Environ., Part A*, 25, 1489–1496.
- Marmorino, G. O., and G. B. Smith (2005), Bright and dark ocean whitecaps observed in the infrared, *Geophys. Res. Lett.*, 32, L11604, doi:10.1029/2005GL023176.
- Melville, W., and P. Matusov (2002), Distribution of breaking waves at the ocean surface, *Nature*, 417, 58–63.
- Monahan, E. (1971), Oceanic whitecaps, *J. Phys. Oceanogr.*, 1, 139–144.
- Monahan, E. (1989), From the laboratory tank to the global ocean, in *The Climate and Health Implications of Bubble-Mediated Sea–Air Exchange*, edited by E. Monahan and M. Van Patten, pp. 43–63, Conn. Sea Grant Coll. Program, Groton.
- Monahan, E. (1993), Occurrence and evolution of acoustically relevant subsurface bubble plumes and their associated, remotely monitorable, surface whitecaps, in *Natural Physical Sources of Underwater Sound*, edited by B. Kerman, pp. 503–517, Springer, New York.

- Monahan, E., and I. G. O'Muircheartaigh (1980), Optimal power-law description of oceanic whitecap coverage dependence on wind speed, *J. Phys. Oceanogr.*, *10*, 2094–2099.
- Monahan, E., and I. O'Muircheartaigh (1986), Whitecaps and the passive remote sensing of the ocean surface, *Int. J. Remote Sens.*, *7*, 627–642.
- Monahan, E., and M. Spillane (1984), The role of oceanic whitecaps in air-sea gas exchange, in *Gas Transfer at Water Surfaces*, edited by W. Brutsaert and G. Jirka, pp. 495–503, Springer, New York.
- Monahan, E., and D. Woolf (1989), Comments on "Variations of whitecap coverage with wind stress and water temperature," *J. Phys. Oceanogr.*, *19*, 706–709.
- Monahan, E., and C. Zietlow (1969), Laboratory comparisons of fresh-water and salt-water whitecaps, *J. Geophys. Res.*, *74*, 6961–6966.
- Monahan, E., C. Fairall, K. Davidson, and P. Boyle (1983a), Observed inter-relationships between 10 m winds, ocean whitecaps and marine aerosols, *Q. J. R. Meteorol. Soc.*, *109*, 379–392.
- Monahan, E., M. Spillane, P. Bowyer, D. Doyle, and P. Stabeno (1983b), Whitecaps and the marine atmosphere, *Rep. 5*, 93 pp., Univ. Coll., Galway, Ireland.
- Monahan, E., M. Spillane, P. Bowyer, M. Higgins, and P. Stabeno (1984), Whitecaps and the marine atmosphere, *Rep. 7*, 103 pp., Univ. Coll., Galway, Ireland.
- Monahan, E., P. Bowyer, D. Doyle, M. Higgins, and D. Woolf (1985), Whitecaps and the marine atmosphere, *Rep. 8*, 124 pp., Univ. Coll., Galway, Ireland.
- Moore, K., K. Voss, and H. Gordon (2000), Spectral reflectance of whitecaps: Their contribution to water-leaving radiance, *J. Geophys. Res.*, *105*, 6493–6499.
- Nordberg, W., J. Conaway, D. Ross, and T. Wilhelm (1971), Measurements of microwave emission from a foam-covered, wind-driven sea, *J. Atmos. Sci.*, *28*, 429–435.
- O'Dowd, C., M. Smith, I. Consterdine, and J. Lowe (1997), Marine aerosol, sea-salt, and the marine sulphur cycle: A short review, *Atmos. Environ.*, *31*, 73–80.
- O'Dowd, C., J. Lowe, M. Smith, and A. Kaye (1999), The relative importance of non-sea-salt sulphate and sea-salt aerosol to the marine cloud condensation nuclei population: An improved multi-component aerosol-cloud droplet parameterization, *Q. J. R. Meteorol. Soc.*, *125*, 1295–1313.
- Pandey, P., and R. Kakar (1982), An empirical microwave emissivity model for a foam-covered sea, *IEEE J. Oceanic Eng.*, *7*, 135–140.
- Piazzola, J., P. Forget, and S. Despiou (2002), A sea spray generation function for fetch-limited conditions, *Ann. Geophys.*, *20*, 121–131.
- Pinet, P. (1992), *Oceanography*, 571 pp., West, St. Paul, Minn.
- Raiter, V., and E. Sharkov (1982), Electrodynamic description of densely packed dispersed systems, *Radio Phys. Quantum Electron.*, *24*, 553–557.
- Reising, S., W. Asher, L. Rose, and M. Aziz (2002), Passive polarimetric remote sensing of the ocean surface: The effects of surface roughness and whitecaps, paper presented at the International Union of Radio Science, URSI Gen. Assem., Maastricht, Netherlands.
- Rose, L. A., W. E. Asher, S. C. Reising, P. W. Gaiser, K. M. St Germain, D. J. Dowgiallo, K. A. Horgan, G. Farquharson, and E. J. Knapp (2002), Radiometric measurements of the microwave emissivity of foam, *IEEE Trans. Geosci. Remote Sens.*, *40*, 2619–2625.
- Rosen, M. (1978), *Surfactants and Interfacial Phenomena*, 295 pp., John Wiley, Hoboken, N. J.
- Rosenkranz, P., and D. Staelin (1972), Microwave emissivity of ocean foam and its effect on nadir radiometric measurements, *J. Geophys. Res.*, *77*, 6528–6538.
- Ross, D., and V. Cardone (1974), Observations of oceanic whitecaps and their relation to remote measurements of surface wind speed, *J. Geophys. Res.*, *79*, 444–452.
- Ross, D., V. Cardone, and J. Conaway Jr. (1970), Laser and microwave observations of sea-surface condition for fetch-limited 17- to 25-m/s winds, *IEEE Trans. Geosci. Electron.*, *8*, 326–336.
- Sander, R., and P. Crutzen (1996), Model study indicating halogen activation and ozone destruction in polluted air masses transported to the sea, *J. Geophys. Res.*, *101*(D4), 9121–9138.
- Scott, J. (1975), The role of salt in whitecap persistence, *Deep Sea Res.*, *22*, 653–657.
- Scott, J. (1986), The effect of organic films on water surface motions, in *Oceanic Whitecaps*, edited by E. Monahan and G. Niocaill, pp. 159–166, Springer, New York.
- Semyonov, B. (1966), Approximate computation of scattering of electromagnetic waves by rough surface contours, *Radio Eng. Electron. Phys.*, *11*, 1179–1187.
- Sievering, H., J. Boatman, E. Gorman, Y. Kim, I. Anderson, G. Ennis, M. Luria, and S. Pandis (1992), Removal of sulfur from the marine boundary layer by ozone oxidation in sea-salt aerosols, *Nature*, *360*, 571–573.
- Sievering, H., E. Gorman, T. Ley, A. Pszenny, M. Springer-Young, J. Boatman, Y. Kim, C. Nagamoto, and D. Wellman (1995), Ozone oxidation of sulfur in sea-salt aerosol particles during the Azores Marine Aerosol and Gas Exchange Experiment, *J. Geophys. Res.*, *100*, 23,075–23,081.
- Smith, P. (1988a), The emissivity of sea foam at 19 and 37 GHz, *IEEE Trans. Geosci. Remote Sens.*, *26*, 541–547.
- Smith, S. (1988b), Coefficients for sea surface wind stress, heat flux, and wind profiles as a function of wind speed and temperature, *J. Geophys. Res.*, *93*, 15,467–15,472.
- Smoot, G., and D. Scott (2000), Cosmic background radiation, in *Review of Particle Physics*, edited by D. Groom et al., *Euro. Phys. J.*, *C15*, 1–6.
- Snyder, R., and R. Kennedy (1983), On the formation of whitecaps by a threshold mechanism. Part I: Basic formalism, *J. Phys. Oceanogr.*, *13*, 1482–1492.
- Snyder, R., L. Smith, and R. Kennedy (1983), On the formation of whitecaps by a threshold mechanism. Part III: Field experiment and comparison with theory, *J. Phys. Oceanogr.*, *13*, 1505–1518.
- Spillane, M., E. Monahan, P. Bowyer, D. Doyle, and P. Stabeno (1986), Whitecaps and global fluxes, in *Oceanic Whitecaps and Their Role in Air-Sea Exchange Processes*, edited by E. Monahan and G. Niocaill, pp. 209–218, Springer, New York.
- Stabeno, P. J., and E. C. Monahan (1986), The influence of whitecaps on the albedo of the sea surface, in *Oceanic Whitecaps and Their Role in Air-Sea Exchange Processes*, edited by E. Monahan and G. Niocaill, pp. 261–266, Springer, New York.
- Stewart, R. (1985), *Methods of Satellite Oceanography*, 360 pp., Univ. of Calif. Press, Berkeley.
- St. Germain, K., G. Poe, and P. Gaiser (2002), Polarimetric emission model of the sea at microwave frequencies and comparison with measurements, *Prog. Electromagn. Res.*, *37*, 1–30.
- Stogryn, A. (1972), The emissivity of sea foam at microwave frequencies, *J. Geophys. Res.*, *77*, 1658–1666.
- Stramska, M., and T. Petelski (2003), Observations of oceanic whitecaps in the north polar waters of the Atlantic, *J. Geophys. Res.*, *108*(C3), 3086, doi:10.1029/2002JC001321.
- Swift, C. (1990), Passive microwave remote sensing of ocean surface wind speed, in *Surface Waves and Fluxes*, vol. II, edited by G. Geernaert and W. Plant, pp. 265–292, Springer, New York.
- Takemura, T., T. Nakajima, O. Dubovik, B. Holben, and S. Kinne (2002), Single-scattering albedo and radiative forcing of various aerosol species with a global three-dimensional model, *J. Clim.*, *15*, 333–352.
- Tans, P., I. Fung, and T. Takahashi (1990), Observational constraints on the global atmospheric CO₂ budget, *Science*, *247*, 1431–1438.
- Taylor, P., and M. Yelland (2001), The dependence of sea surface roughness on the height and steepness of the waves J, *Phys. Oceanogr.*, *31*, 572–590.
- Thorpe, S. (1982), On the clouds of bubbles formed by breaking wind-waves in deep water, and their role in air-sea gas transfer, *Philos. Trans. R. Soc. London, Ser. A*, *304*, 155–210.
- Toba, Y., and M. Chaen (1973), Quantitative expression of the breaking of wind waves on the sea surface, *Rec. Oceanogr. Works Jpn.*, *12*, 1–11.
- Toba, Y., and M. Koga (1986), A parameter describing overall conditions of wave breaking, whitecapping, sea-spray production and wind stress, in *Oceanic Whitecaps Their Role in Air-Sea Exchange Processes*, edited by E. Monahan and G. Niocaill, pp. 37–47, Springer, New York.
- Troitsky, V. (1962), Radio emission of the moon, its physical state, and the nature of its surface, in *The Moon*, edited by Z. Kopal and Z. Mikhailov, pp. 475–489, Elsevier, New York.
- Ulaby, F., R. Moore, and A. Fung (1986), *Microwave Remote Sensing: Active and Passive, From Theory to Applications*, vol. III, 2162 pp., Book-Mart, North Bergen, N. J.
- Villarino, R., A. Camps, M. Vall-Ilossera, J. Miranda, and J. Arenas (2003), Sea foam effects on the brightness temperature at L-band, in *Proceedings of Geoscience and Remote Sensing Symposium (IGARSS '03)*, vol. 5, pp. 3076–3078, IEEE Press, Piscataway, N. J.
- Wang, Q., E. Monahan, W. Asher, and P. Smith (1995), Correlations of whitecap coverage and gas transfer velocity with microwave brightness temperature for plunging and spilling breaking waves, in *Air-Water Gas Transfer*, edited by B. Jähne and E. Monahan, pp. 217–225, Aeow, Hanau, Germany.
- Wanninkhof, R. (1992), Relationship between wind speed and gas exchange over the ocean, *J. Geophys. Res.*, *97*, 7373–7382.
- Webster, W., Jr., T. Wilhelm, D. Ross, and P. Gloersen (1976), Spectral characteristics of the microwave emission from a wind-driven foam-covered sea, *J. Geophys. Res.*, *81*, 3095–3099.
- Wentz, F. (1974), The effect of surface roughness on microwave sea brightness temperatures, *Contractor Rep. 3-35345*, NOAA, Silver Spring, Md.
- Wentz, F. (1983), A model function for ocean microwave brightness temperature, *J. Geophys. Res.*, *88*, 1892–1908.

- Wentz, F. (1992), Measurement of oceanic wind vector using satellite microwave radiometers, *IEEE Trans. Geosci. Remote Sens.*, *30*, 960–972.
- Wentz, F. (1997), A well-calibrated ocean algorithm for special sensor microwave/imager, *J. Geophys. Res.*, *102*, 8703–8718.
- Wentz, F., and E. Francis (1992), Nimbus-7 SMMR ocean products, 1979–1984, *RSS Tech. Rep. 033192*, Remote Sens. Syst., Santa Rosa, Calif.
- Wentz, F., E. Christensen, and K. Richardson (1980), Dependence of sea surface emissivity on friction velocity as derived from SMMR/SASS, in *Oceanography From Space*, vol. 13, *Marine Science*, edited by J. Gower, pp. 741–749, Springer, New York.
- Whitlock, C., D. Bartlett, and E. Gurganus (1982), Sea foam reflectance and influence on optimum wavelength for remote sensing of ocean aerosols, *Geophys. Res. Lett.*, *9*, 719–722.
- Wilheit, T. (1978), A review of applications of microwave radiometry to oceanography, *Boundary Layer Meteorol.*, *13*, 277–293.
- Wilheit, T. (1979), A model for the microwave emissivity of the ocean's surface as a function of wind speed, *IEEE Trans. Geosci. Electron.*, *17*, 244–249.
- Wilheit, T., A. Chang, and A. Milman (1980), Atmospheric corrections to passive microwave observations of the ocean, *Boundary Layer Meteorol.*, *18*, 65–77.
- Williams, G., Jr. (1969), Microwave radiometry of the ocean and the possibility of marine wind velocity determination from satellite observations, *J. Geophys. Res.*, *18*, 4591–4594.
- Williams, G., Jr. (1971), Microwave emissivity measurements of bubbles and foam, *IEEE Trans. Geosci. Electron.*, *9*, 221–224.
- Winter, B., and P. Chýlek (1997), Contribution of sea salt aerosol to the planetary clear-sky albedo, *Tellus, Ser. B*, *49*, 72–79.
- Wu, J. (1979), Oceanic whitecaps and sea state, *J. Phys. Oceanogr.*, *9*, 1064–1068.
- Wu, J. (1988), Variations of whitecap coverage with wind stress and water temperature, *J. Phys. Oceanogr.*, *18*, 1448–1453.
- Wu, J. (1992a), Bubble flux and marine aerosol spectra under various wind velocities, *J. Geophys. Res.*, *97*, 2327–2333.
- Wu, J. (1992b), Individual characteristics of whitecaps and volumetric description of bubbles, *IEEE Trans. Oceanic Eng.*, *17*, 150–158.
- Xu, D., X. Liu, and D. Yu (2000), Probability of wave breaking and whitecap coverage in a fetch-limited sea, *J. Geophys. Res.*, *105*, 14,253–14,259.
- Yueh, S. (1997), Modeling of wind direction signals in polarimetric sea surface brightness temperatures, *IEEE Trans. Geosci. Remote Sens.*, *35*, 1400–1418.
- Zhang, M., and J. Johnson (2001), Comparison of modeled and measured second azimuthal harmonics of ocean surface brightness temperatures, *IEEE Trans. Geosci. Remote Sens.*, *39*, 448–452.
- Zhao, D., and Y. Toba (2001), Dependence of whitecap coverage on wind and wind-wave properties, *J. Oceanogr.*, *57*, 603–616.

M. D. Anguelova, Remote Sensing Division, Code 7223, Naval Research Laboratory, 4555 Overlook Avenue, SW, Washington, DC 20375-5320, USA. (magda@nrl.navy.mil)

F. Webster, College of Marine Studies, University of Delaware, Lewes, DE 19958, USA.